Geological Society of America
Special Paper 360
2002

Crustal structure of the Bering and Chukchi shelves: Deep seismic reflection profiles across the North American continent between Alaska and Russia

Simon L. Klemperer*
Department of Geophysics, Stanford University, Stanford, California 94305-2215, USA
Elizabeth L. Miller
Arthur Grantz
Department of Geological and Environmental Sciences, Stanford University, Stanford, California 94305-2115, USA
David W. Scholl
Department of Geophysics, Stanford University, Stanford, California 94305-2215, USA
Bering-Chukchi Working Group†

ABSTRACT

In 1994, 3750 km of crust-penetrating marine seismic-reflection profiles were acquired across the North American continent from the Aleutian basin to the Arctic Ocean. The two subparallel profiles cross the Bering and Chukchi shelves, passing through the Bering Strait between Russia and Alaska. The 40-fold, ≥15-s-penetration reflection data clearly image the major offshore sedimentary basins, lower-crustal layering, the reflection Moho, and rare sub-Moho reflectors.

The crust beneath the northern and southern segments is relatively nonreflective compared to the central part. By inference from onshore geology we associate the northern region, the Chukchi Shelf and Beaufort margin, with the Arctic Alaska–Chukotka cratonic block, and the southern region, the Outer Bering Shelf, with displaced continental and magmatic arc terranes. The central segment, extending from north of the Bering Strait to the Inner Bering Shelf south of Saint Lawrence Island, has distinctive highly reflective crust that we associate with plutonism in the middle to Late Cretaceous Okhotsk-Chukotsk magmatic belt and, in particular, with structures developed during its contemporaneous extensional history.

The reflection Moho is visible at traveltimes as great as 13.5 s (~39 km depth) beneath the Barrow Arch where sedimentary rocks are ~20 km thick. The Moho is at traveltimes as great as 13 s (~40 km?) beneath the Saint Matthew–Nunivak arch, a

*Corresponding author. E-mail: sklemp@stanford.edu.
†The Bering-Chukchi Working Group includes Jon R. Childs (U.S. Geological Survey, 345 Middlefield Road, Menlo Park, California 94025, USA), Nikita A. Bogdanov (Institute of the Lithosphere, Staromonelny Perevlok, 22 Moscow, 109180, Russia), Igor N. Belykh (Institute of Marine Geology and Geophysics, Yuzhno-Sakhalinsk, Russia; current address, Engineering Geophysics Company, Sakhalin, Russia), Helios Gnibidenko (Shirshov Institute of Oceanology, Moscow, 117851, Russia [deceased]), Brian Galloway (Department of Geophysics, Stanford University, Stanford, California 94305-2215; current address, Hewlett-Packard, 1501 Page Mill Road., MS 5LA, Palo Alto, California 94304, USA), Brian Hicks (Department of Geophysics, Stanford University, Stanford, California 94305-2215; current address, 2342 Yale Street, Palo Alto, California 94306, USA), Frances Cole (Department of Geological and Environmental Sciences, Stanford University, Stanford, California 94305-2115; current address, U.S. Department of Energy, National Energy Technology Laboratory, Morgantown, West Virginia 26507-0880, USA), and Jaime Toro (Department of Geological and Environmental Sciences, Stanford University, Stanford, California 94305-2115; current address, Department of Geology and Geography, West Virginia University, Morgantown, West Virginia 26506-6300, USA).

Klemperer, S.L., Miller, E.L., Grantz, A., Scholl, D.W., and the Bering-Chukchi Working Group, 2002, Crustal structure of the Bering and Chukchi shelves: Deep seismic reflection profiles across the North American continent between Alaska and Russia, *in* Miller, E.L., Grantz, A., and Klemperer, S.L., eds., Tectonic Evolution of the Bering Shelf–Chukchi Sea–Arctic Margin and Adjacent Landmasses: Boulder, Colorado, Geological Society of America Special Paper 360, p. 1–24.

broad basement high underlain by Mesozoic and Paleogene arc rocks. The reflection Moho is visible at traveltimes as short as 10 s (32 km Moho depth according to refraction recordings) in the Bering Strait where crystalline basement is at the seafloor. It is at 11 s beneath the Navarin Basin, where the thickness of Tertiary strata is as much as ~8 km, indicating a likely crustal thickness of <25 km.

INTRODUCTION

The seismic profiles presented in this chapter (Fig. 1; for a more detailed location map see Plate 1 of the Preface) form the first continuous deep seismic reflection transect across the North American continent, and provide a first regional look at the entire crust of the Bering and Chukchi shelves between Alaska and northeastern Russia. The history of these regions is the composite result of the convergent and accretionary tectonics of the North Pacific rim and the extensional tectonics that began to form the Arctic Ocean in the Jurassic. For many years political and language barriers created artificial boundaries between Alaska and Russia. In actuality this region represents a single tectonic plate that includes parts of both North America and Russia (Mackey et al., 1997), and geologic units associated with the convergent and accretionary history of the Pacific margin and the North American Cordillera continue uninterrupted from Alaska to Russia (e.g., Nokleberg et al., 2000; Miller et al., this volume, Chapter 17). Hence, one of the most prominent puzzles presented by the geology of this region is why does the high topography of the North American Cordillera that extends from Mexico to Alaska diminish in the Bering Strait region?

The sedimentary basins in the Bering-Chukchi region have been explored for hydrocarbons by seismic surveys and exploratory wells (e.g., Craig et al., 1985; Turner et al., 1985, 1986; Thurston and Theiss, 1987; Scholl et al., 1987a; Worrall, 1991; Sherwood et al., this volume). In contrast, little was known (scattered well penetrations and a few dredge sites along the Beringian shelf edge; Plate 1, Miller et al., this volume, Preface) about the vast area of submerged continental crust that constitutes the older basement for these basins.

In this chapter a brief geological overview (organized from north to south) is followed by a review of previous crustal studies in the region and a description of our seismic data acquisition and processing. The main part of the paper presents a description and interpretation of significant reflections recorded along our seismic transect from north to south, including identification of the major sedimentary sequences, and a comparison of Moho reflections with existing refraction and potential field data. Interpretation of crustal type based on reflective character is also discussed.

GEOLOGIC OVERVIEW

The geologic history of Alaska (e.g., Plafker and Berg, 1994a) can be described by the progressive southward growth of continental crust by accretion and imbrication of continental-margin and oceanic sediments, allochthonous terranes, and magmatic arc systems and ophiolitic rocks that compose southern and central Alaska against a more rigid lithospheric block represented by the Arctic Alaska superterrane of northern Alaska. Although it is not apparent from surface geologic relations, the deep seismic data indicate that the Bering and Chukchi shelves (Fig. 1; e.g., see Scholl et al., 1987a; Plate 1, Miller et al., this volume, Preface) can be divided into three main parts with distinct crustal structure and crustal histories. These are shown schematically in Figure 1 (inset) as (1) Arctic Alaska–Chukotka plate, (2) mid-Cretaceous magmatic belt, and (3) Paleogene arc and displaced terranes.

1. The northern region consists of a displaced (rotated) fragment of the North American craton, the Arctic Alaska–Chukotka microplate, and overlying Proterozoic-to-Cenozoic sedimentary cover rocks. This area includes the offshore Chukchi and Beaufort shelves, the North Slope of Alaska, most of the Brooks Range, and the northern part of northeastern Rus-

Figure 1. Location map for Bering and Chukchi shelves. Heavy solid line from south to north (S–N): EW 94–10 deep seismic reflection tracklines shown in this chapter as line drawing (Fig. 2) and stack data (Plate 2). Numbers (0–9) are distances in hundreds of kilometers north and south of Bering Strait. Shotpoint numbers are given in Plate 1 of Miller et al., this volume, Preface. Heavy dashed line marked EW 94–10 indicates seismic reflection tracklines acquired in this experiment but not shown in this paper, including circle over Kotzebue Arch and dogleg southeast of Saint Lawrence Island, both shot in bad weather. Fine dashed lines marked EW 94–09 indicate deep reflection profiles acquired during preceding cruise EW 94–09 (McGeary et al., 1994). Dotted line marked Cooper et al. shows location of sonobuoy-refraction and gravity profile of Cooper et al. (1987). Dotted line marked Tolson shows location of industry reflection profile of Tolson (1987b, p. 131). Squares are land seismic stations that recorded onshore-offshore seismic data during cruises EW94–09 and EW94–10 (Saint Lawrence and north, Wolf et al., this volume; Cape Newenham and south, Fliedner and Klemperer, 1999, 2000). Offshore bathymetry is unshaded <200 m; shading density increases at 2000 and 4000 m. Offshore basins: sedimentary fill (Cenozoic south of Herald Arch, post-Devonian north of Herald Arch) is shaded where >3 km, and contoured at 2 km intervals (Kirschner, 1988, except Anadyr Basin: Worrall, 1991). Black circles (North Slope, Kotzebue, Norton, and Navarin Basins) are wells mentioned in text or figures, with identifying letters (north to south): B is South Barrow #1 (Collins, 1961); To is Topagoruk test well 1 (Collins, 1958); Pe is Peard #1; Tu is Tunalik #1 (Sherwood et al., this volume); PN is Point Nimiuk #1; CE is Cape Espenberg #1; No1 and No2 are Norton Sound COST#1 and COST#2; Na1 is Navarin Basin COST#1 (Plate 1). Gray ellipse (Seward Peninsula) and circle (Chukotka Peninsula) are schematic locations of gneiss domes. South Anyui suture is after Worrall (1991). Inset shows mid-Cretaceous magmatic belt after Miller et al. (this volume, Chapter 17).

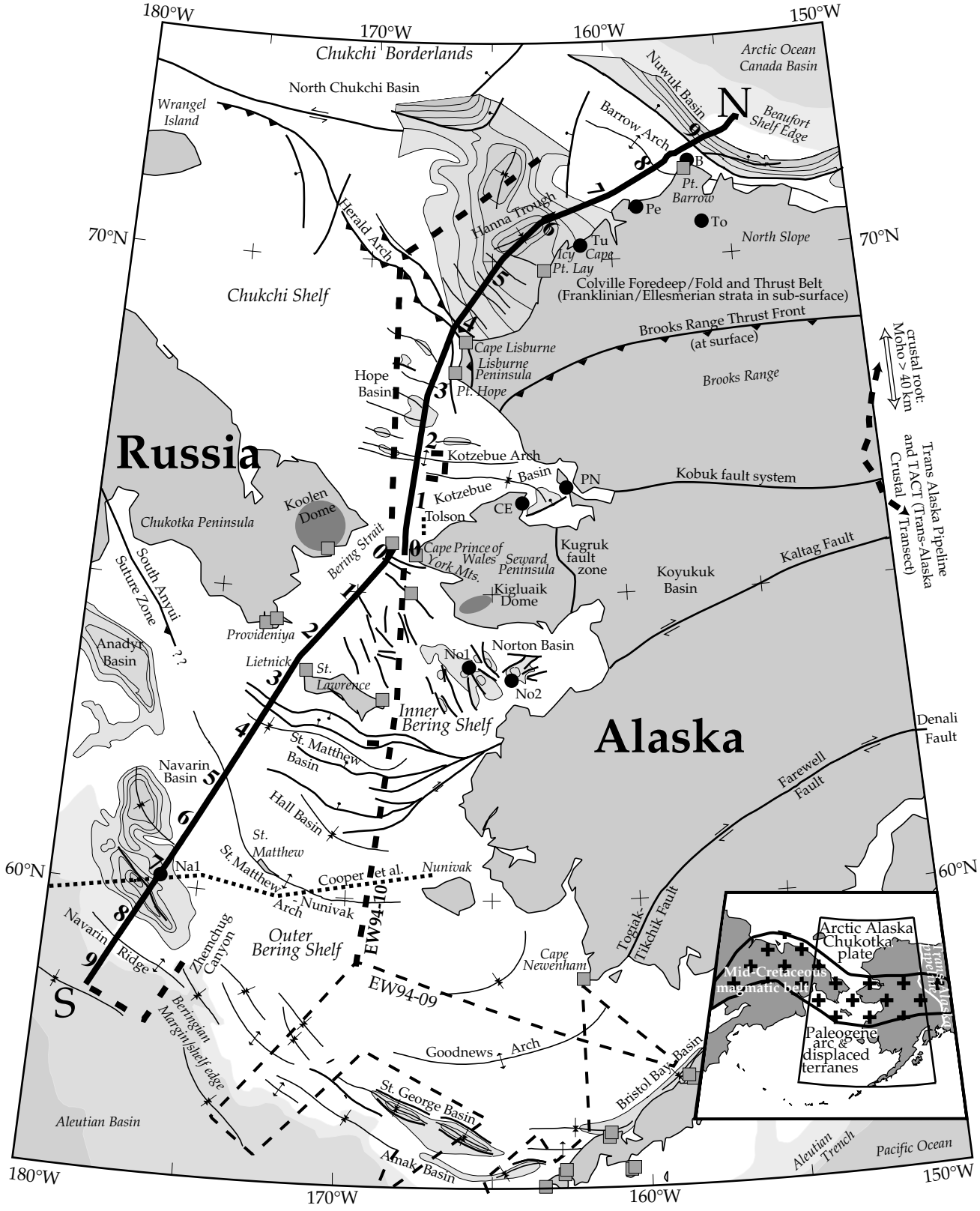

sia (e.g., Moore et al., 1994; Nokleberg et al., 2000). It is bounded on the north by oceanic crust of the Arctic Ocean.

2. The central region consists of the Inner Bering Shelf from north of the Bering Strait to south of Saint Lawrence Island, and includes the internal or southern portion of the Brooks Range orogen, the Yukon-Koyukuk region of interior Alaska, and the Seward Peninsula. Thick sequences of deformed middle to Late Cretaceous marine and paralic sedimentary rocks characterize the Yukon-Koyukuk region, which is underlain by accreted oceanic sediments and island-arc rocks and intruded by middle to Late Cretaceous (118–80 Ma) plutons (Patton et al., 1994; Nokleberg et al., 2000; Miller et al., this volume, Chapter 17). This region is inferred to have undergone variable, but locally high, amounts of extension in the Cretaceous (e.g., Miller and Hudson, 1991; Pavlis et al., 1992; however, this interpretation is not shared by all, e.g., Till et al., 1993).

3. The southern region consists of the Outer Bering Shelf, formed of continental and arc terranes assembled along transpressional fault boundaries or formed in place during Cretaceous-Paleogene convergence and strike-slip motion along the North Pacific rim. New arc material was intruded into preexisting continental material, some of Precambrian age, but largely much younger than the Arctic Alaska–Chukotka microplate to the north. Plate-boundary motion along the Beringian margin (the foot of the continental slope of the Bering Shelf) between the Kula oceanic and North American continental lithosphere ended in the early Eocene. Magmatism, subduction, and plate-boundary deformation jumped south at ca. 56 Ma from the Beringian margin to the Aleutians, trapping what is probably the former oceanic Kula plate to form the Aleutian basin of the Bering Sea (e.g., Cooper et al., 1987; Scholl et al., 1987b).

The following descriptions of the geology of these three regions or crustal provinces focus on geologic relations closest to the line of our seismic transect (line S–N in Fig. 1).

Northern region: Chukchi Shelf, Brooks Range, Herald Arch, and Hope Basin

The northern continental margin of Alaska and the Chukchi Shelf is the Beaufort passive margin, formed by Neocomian rifting and earliest Aptian (121 Ma) seafloor spreading in the Canada Basin as the Arctic Alaska–Chukotka microplate rotated counterclockwise away from the formerly contiguous North American craton (Lawver and Scotese, 1990; Embry, 1990; Grantz et al., 1990, 1998; Mickey et al., this volume; but see Lane, 1997, for a contrary model). The oldest beds at the base of the Cretaceous and Tertiary passive margin sequence of the Canada Basin on the Barrow Arch, its southern rift shoulder, are Hauterivian pelagites. This sequence progrades and thickens northward into the Canada Basin, and thins rapidly southward onto the Barrow Arch (Fig. 1). There it overlaps the northern part of an older south-facing sequence of paralic and marine stable shelf deposits of the Upper Devonian to lower Lower Cretaceous Ellesmerian sequence (Grantz et al., 1987; Plafker and Berg, 1994b) and, beneath a major Devonian unconformity, the underlying Ordovician and Silurian Franklinian sequence.

The upper Ellesmerian sequence consists of Jurassic marine clastic strata derived largely from the Barrow Arch, and the coeval Dinkum succession, deposited in the Dinkum rift-margin graben system on the north flank of the Barrow Arch (Grantz et al., 1990) during the early, prebreakup stages of rifting of the Canada Basin. The lower Ellesmerian sequence in northern Alaska consists of Lower Mississippian clastic rocks (Endicott Group) and Upper Mississippian to Triassic marine carbonates and clastic strata sourced in the Canadian Arctic Islands, from which they are now separated by the oceanic Canada Basin of the Arctic Ocean. The deepest part of this sequence could be Late Devonian. In the Topagoruk-1 test well (To in Fig. 1; Collins, 1958), the base of the Ellesmerian overlies with angular unconformity steeply dipping conglomerate and carbonaceous shale of Middle (Early?) Devonian age. Regional relations suggest that these beds unconformably overlie Ordovician and Silurian distal turbidites and graptolitic hemipelagites of the Franklinian sequence (usage after Lerand, 1973). This unconformity was attributed to the Ellesmerian orogeny by Moore et al. (1994), but Trettin (1991) considered the Ellesmerian orogeny to be latest Devonian–Early Carboniferous [Mississippian] in their type area in the Canadian Arctic Islands, so the unconformity correlates better with the Scandian phase of the Caledonian orogeny (late Early Silurian to Early Devonian [McKerrow et al., 2000]). During the Ordovician, Chukotka was separated from Arctic Alaska by a strait that connected the Iapetus Ocean and the paleo–Pacific Ocean, and was sutured to western Arctic Alaska in the Early Silurian (Nokleberg et al., 2000).

The south-facing passive continental margin of the Arctic Alaska microplate was deformed by north-vergent thrust faults during Middle or Late Jurassic to Early Cretaceous time, marking the closure of the Angayucham Ocean (Mayfield et al., 1988; Wirth and Bird, 1992; Moore et al., 1994). This compressional orogeny was succeeded by large-magnitude mid-Cretaceous extension or orogenic collapse (Miller and Hudson, 1991). The southern boundary of the Arctic Alaska–Chukotka plate is typically depicted in Russia as the South Anyui suture zone (Fujita and Newberry, 1982; Sokolov et al., this volume), and in Alaska it is placed along a large positive magnetic anomaly near the southern boundary of the modern Brooks Range (approximately along the younger Kobuk fault zone in Fig. 1). The anomaly marks the position of the updip end of a complex thrust sheet that contains the Upper Devonian to Lower Jurassic oceanic rocks of the Angayucham terrane (Grantz et al., 1991; Moore et al., 1994). On the basis of the analysis of Miller and Hudson (1991), the root zone or internides of the Brooks Range orogen (as distinct from the crustal root beneath the modern topography of the Brooks Range) must have extended an unknown distance south beneath what is now the Koyukuk basin.

The modern Brooks Range consists of a series of complexly deformed thrust sheets emplaced onto continental crust and continental-margin facies sedimentary rocks of the Arctic Alaska

plate (Fuis et al., 1995). After Jurassic and Early Cretaceous thrust faulting, the Brooks Range shed large volumes of clastic debris northward into the Cretaceous-Tertiary Colville foredeep, which extends offshore onto the Chukchi Shelf (Grantz and May, 1987). Its sedimentary rocks are deformed by thrusting in the foreland of the Brooks Range fold and thrust belt in both the northern foothills of the Brooks Range and the eastern Chukchi Shelf (Moore et al., 1994). A thick Aptian-Cenomanian sedimentary section present beneath the western Colville Basin and the southern part of the Hanna Trough, referred to as the Corwin Delta, was derived from a western source area located beneath the Hope Basin and its environs (Moore et al., 1994). The Corwin Delta implies that significant topography, and hence a root to the Brooks Range, must have characterized this area in the Early Cretaceous, and that subsequent extension and collapse were required to drop the Hope Basin and its environs below sea level. Beneath the eastern Chukchi Shelf the southern margin of the Colville Basin is deformed by numerous thrust faults that are splays of the Late Cretaceous–Paleogene northeast-directed Herald thrust belt (Grantz and May, 1987). In the Lisburne Hills of westernmost Alaska, and perhaps beneath the Chukchi Shelf, this thrust belt may be superimposed on a mid-Cretaceous continuation of the Brooks Range orogen (Moore et al., this volume). Today the Herald Arch disappears southward, and the Brooks Range disappears westward, beneath the Eocene and younger deposits of the Hope Basin (Tolson, 1987a), which appears to be a transtensional basin geometrically linked to right-lateral displacement along the Kobuk fault zone (e.g., Tolson, 1987a; Worrall, 1991).

Central region: Bering Strait, Saint Lawrence Island, and Inner Bering Shelf

A broad basement high in the region around the Bering Strait and Saint Lawrence Island links the Chukotka Peninsula of Russia to the Seward Peninsula of Alaska (Fig. 1). East of the Seward Peninsula, across the Kugruk fault zone—an uncertain strike-slip or normal fault (Till and Dumoulin, 1994; Plafker and Berg, 1994b)—and south of the Brooks Range and the Kobuk fault system (Fig. 1) are mainly Cretaceous marine clastic sequences of the Koyukuk Basin. The basin is inferred to depositionally overlie the collapsed and extended root zone of the Brooks Range orogen (Miller and Hudson, 1991). The Seward Peninsula exposes mostly greenschist-facies slates, schists, marbles, and greenstone that locally preserve evidence for an older blueschist metamorphism (Till and Dumoulin, 1994). These are overprinted by biotite to granulite facies metamorphism of Cretaceous age in a series of gneiss domes such as the Kigluaik gneiss dome (Fig. 1; Amato et al., this volume; Akinin and Calvert, this volume) and are intruded by mid–Late Cretaceous plutons. Less metamorphosed lower Paleozoic carbonates underlie the York Mountains on the western tip of the Seward Peninsula (Fig. 1) (Till and Dumoulin, 1994).

Small exposures of Paleozoic and early Mesozoic rocks occur on Saint Lawrence Island and have been correlated to shelfal facies in thrust sheets of the Arctic Alaska superterrane and the overthrust Angayucham terrane in the Brooks Range of northern Alaska (Patton and Csejtey, 1980). These exposures are unconformably overlain by Cretaceous and early Paleocene volcanic rocks of intermediate composition and are intruded by Cretaceous plutons (Patton et al., 1976). The Cretaceous igneous rocks are part of a 6000-km-long mid-Cretaceous to locally Paleocene magmatic belt that is well developed in Russia and includes the Okhotsk-Chukotsk volcanic belt. Magmatism is believed to be at least partly related to subduction beneath the North Pacific margin, possibly above a southward-retreating subduction zone (Rubin et al., 1995; Amato and Wright, 1997; Bering Strait Geologic Field Party, 1997; Miller et al., this volume, Chapter 17; Amato et al., this volume). Late Cretaceous (65–77 Ma) and early Tertiary (61 Ma) arc magmatic rocks presumably linked to the Okhotsk-Chukotsk volcanic belt are found on Saint Matthew Island (Patton et al., 1976) and in dredge samples from the continental slope (Davis et al., 1989). On the Chukotka and Seward Peninsulas, Cretaceous magmatism was contemporaneous with ductile thinning and uplift of mid-crustal rocks in the Koolen and Kigluaik gneiss domes (Amato et al., this volume; Akinin and Calvert, this volume). These gneiss domes, or metamorphic culminations, involve Paleozoic and possibly older protoliths and are the result of extension within the magmatic belt and the overthickened root of the Brooks Range orogen.

Although most of the erosion and uplift of the Seward Peninsula (and by inference the Bering Strait basement high) occurred during the Cretaceous (Dumitru et al., 1995), modest onshore erosion and offshore formation of the Norton, Hope, and Saint Matthew–Hall basins starting in the Eocene testify to an extensional to transtensional environment in this region during the early Tertiary (Cooper et al., 1987; Marlow et al., 1987; Tolson, 1987a, 1987b; Worrall, 1991). Mild north-south extension and an unknown amount of strike-slip motion has continued to the present, as indicated by development of the Neogene Bering Sea basaltic province (Moll-Stalcup, 1994; Akinin et al., 1997) and normal-fault focal mechanisms from the Seward and Chukotka Peninsulas (Mackey et al., 1997; Fujita et al., this volume). The Quaternary basalt flows and cinder cones scattered across this portion of the transect (Moll-Stalcup, 1994; Wirth et al., this volume) extend to the Beringian shelf edge, as shown by exposures on the Pribilof Islands and dredge samples recovered from the continental margin near the Navarin Basin (Davis et al., 1993).

Southern region: Outer Bering Shelf

The Outer Bering Shelf is inferred to be underlain mostly by accreted terranes of the North Pacific, as suggested by rock units exposed in Alaska south of the Brooks Range and Seward Peninsula (Fig. 1), as well as Late Cretaceous and early Paleogene arc sequences. In a process beginning with the closing of

the Angayucham Ocean, from Late Jurassic to early Eocene time, the ancestral circum-Pacific subduction zone migrated southward from a location beneath the Inner Bering Shelf to the modern Beringian shelf edge, and volcanism occurred in a broad subaerial magmatic belt during highly oblique subduction (Worrall, 1991). Saint Matthew Island, located between our two seismic transects (Fig. 1), is composed almost entirely of Paleogene igneous rock (Patton et al., 1976; Moll-Stalcup, 1994). Cenozoic and older terranes, developed at more southerly latitudes, were transported an unknown distance and subsequently accreted during the Late Cretaceous and Paleogene to southern and western Alaska by transpression along major dextral structures (Jones et al., 1977; Coney and Jones, 1985; Plafker and Berg, 1994b; Nokleberg et al., 2000). Dredge samples and seismic data show that the outermost Bering Shelf to at least long 174°W is composed of Peninsular terrane rocks (Naknek Formation) that may extend all the way to the Navarin Ridge (Marlow and Cooper, 1980; Jones et al., 1981; Worrall, 1991).

Major dextral features such as the Kaltag and the Farewell faults (Fig. 1) postdate the era of terrane accretion, which was mostly middle Cretaceous in the area of these faults. It remains a matter of debate whether these faults (1) ever extended across the entire Bering Shelf from northeast to southwest (e.g., Scholl and Stevenson, 1989); (2) rotate to form, or are truncated by, the postulated post-middle Eocene northwest-southeast transform trend parallel to the Beringian margin (e.g., Worrall, 1991); or (3) splay and die out under the Inner Bering Shelf beneath the Norton Basin (the Kaltag fault) or in southwestern Alaska (the Farewell fault).

The Beringian margin transform or highly oblique subduction zone was abandoned when subduction jumped southward to the modern Aleutian arc in the early Eocene (ca. 50–55 Ma), trapping most likely Kula plate oceanic crust between the Bering margin and the new arc to form the modern Aleutian basin of the Bering Sea in the process (Scholl et al., 1987b). Following this transition, transtension is thought to have continued to affect the outer edge of the Bering Shelf, forming a series of deep and elongate sedimentary basins, including the Bristol Bay, Saint George, and Navarin Basins (Cooper et al., 1987; Worrall, 1991). The largest and deepest of these, the Navarin Basin, contains to 12 km of late Eocene and younger strata (Worrall, 1991).

PREVIOUS CRUSTAL STRUCTURE STUDIES

Our only detailed knowledge of the deep-crustal structure of Alaska comes from the Trans-Alaska Crustal Transect (TACT) seismic profiles acquired intermittently along the Trans-Alaska Pipeline (Fig. 1), east of our marine transect. The TACT wide-angle reflection-refraction profile between the Kaltag fault and the Denali fault at 64°–65°N, 1000 km east of our marine profiles (Beaudoin et al., 1992) (Fig. 1), shows a thin crust, only ~30 km thick, with a low average velocity, ~6.1 km/s. Beaudoin et al. (1992) noted that this crust of the Yukon-Tanana terrane is clearly reflective from ~10 to 27 km depth (equivalent to ~3.5–9 s). Although their wide-angle data cannot be directly compared to our reflection profiles, their data require velocity layering that is 0.2–0.5 km thick, a scale that would also be strongly reflective on our marine reflection profiles. Both the region of central Alaska sampled by the TACT transect and the central region of our marine transect are within the middle to Late Cretaceous magmatic belt defined by Miller et al. (this volume, Chapter 17). According to Pavlis et al. (1992), the Yukon-Tanana terrane of central Alaska was thinned by a factor of 2 to 4 during mid-Cretaceous extension, although as much as half of the modern crustal thickness may represent subsequent tectonic or magmatic underplating.

The TACT refraction profile across the Brooks Range (Fuis et al., 1995) extends from just south of the Kobuk fault to the North Slope at ~69°N, 800 km east of our marine transect (Fig. 1). Crustal thickness is ~37 km at the north and south ends of the profile, but Fuis et al. (1995) recognized a >100-km-wide zone of crustal thickening, the Moho depth being 50 km beneath the highest modern topography of the Brooks Range (Fig. 1). The collocated TACT low-fold near-vertical reflection profile shows that the Brooks Range is characterized by south-dipping thrust duplexes in the upper crust, overlying in turn a poorly reflective middle to lower crust, and a basal-crustal reflective layer ~5 km thick (Fuis et al., 1995). The poorly reflective middle crust of the Arctic Alaska microplate is 30 km thick beneath the North Slope, but thins south beneath the Brooks Range allochthons, apparently forming a crustal-scale wedge between the allochthons and the basal reflective layer. On the basis of this interpretation of the reflection character of the TACT profile, the southern limit of the Arctic Alaska microplate that is autochthonous with respect to Brooks Range orogenesis is at about the southern limit of the crustal root shown schematically in Figure 1. South of the modern Brooks Range, the crust appears to lack the less-reflective middle crust. The data of Fuis et al. (1995, their Fig. 2a) suggest that the crust below the Koyukuk basin is continuously reflective from 4 to 12 s, although their low-fold data acquisition makes it difficult to directly compare their data with our conventional reflection profiles.

Knowledge of the crustal structure of far-eastern Russia is rudimentary, and no active-source deep-crustal profiles have been recorded. Mackey et al. (1998) used regional earthquake recordings to model a 37 km crustal thickness at long 160°E, lat 62°–65°N. Older Russian studies of converted earthquake phases summarized by Wolf et al. (this volume) suggest crustal thicknesses of 32–39 km in the Chukotka Peninsula.

Although the sedimentary basins of the continental shelves between Russia and Alaska have been extensively explored for potential hydrocarbon reserves by seismic-reflection studies (e.g., Craig et al., 1985; Thurston and Theiss, 1987; Scholl et al., 1987a; Worrall, 1991), no crustal-penetrating profiles had been acquired, despite attempts by Cooper et al. (1987), prior to those described herein and by Wolf et al. (this volume). A regional surface-wave model of Jin and Herrin (1980) provides an average crustal thickness of 28 km for the Bering Shelf, a value that

masks the considerable lateral variation shown here. Cooper et al. (1987) combined upper-crustal refraction velocities with gravity modeling to suggest crustal thicknesses in the Outer Bering Shelf ranging from 20 km beneath the Navarin Basin to 43 km beneath the Saint Matthew–Nunivak arch, but such values depend strongly on assumed densities.

ACQUISITION, PROCESSING, AND INTERPRETATION OF SEISMIC DATA

The RV *Maurice Ewing,* operated by Lamont-Doherty Earth Observatory on behalf of the University National Oceanographic Laboratory Systems, acquired 3750 km of seismic data (Fig. 1) using a 4 km, 160 channel streamer and a 20 gun, 8355 in^3 airgun source. The shot interval was either 50 m (yielding 40-fold data) or 75 m (27-fold data), the larger interval being used along line segments where strong currents prevented full recording times with 50 m shot spacing. Record lengths varied from 15 s to 23 s. Absolute shot times were recorded to enable subsequent analysis of the seismic signals recorded at offsets from 10 to >250 km at 11 land sites in Alaska and Russia around the Bering Strait and on the northwestern coast of Alaska (Fig. 1; Brocher et al., 1995; Wolf et al., this volume). Gravity and magnetic data (Fig. 2) and sonobuoy and 3.5 kHz echo-sounder data were also acquired along the tracklines.

A composite reflection profile from the Aleutian basin to the Arctic Ocean (S–N in Fig. 1) is shown as an annotated line-drawing (Fig. 2) and as an interpreted stack section (Plate 2). The seismic data were processed by CTC Pulsonic, now part of Scott-Pickford, Inc., following the processing sequence listed in Plate 2. Interpretations described in the text were made on 1:100 000 scale stack sections, then transferred to the 1:400 000 scale sections of Plate 2. Greater detail is evident on the 1:100 000 scale sections than on the reduced-scale sections of Plate 2, because of the small scale of reproduction and because the data in Plate 2 have been low-pass filtered and trace summed to match the resolution of the seismic data to that of the printing process at small scales (e.g., Klemperer and Hobbs, 1991). Our seismic data are shown as unmigrated time sections, so interpreters must be aware of the need to convert time to depth in a nonlinear way dependent on the velocity structure of the Earth, and must recognize that dipping reflections have lower dips and are downdip of the reflectors that produced them (e.g., Klemperer and Hobbs, 1991).

An important limitation on comparisons of different segments of our reflection profiles is the inevitable variability in reflection quality due to varying weather and sea state, partial equipment failure or changes in acquisition parameters, and perhaps most important, to changes in seafloor conditions. The region where our data quality suffered most from poor weather is near the Kotzebue Arch. Data from km +100 to +145 (in Plate 2 distances are given north [positive km] and south [negative km] of the Bering Strait) were acquired as a gale developed, causing noise on the recording streamer; data from km +145 to +200 were acquired after a 24 h delay as the gale abated. Fortunately, data from the parallel profile acquired ~40 km to the west 1 week later in good weather provide confirmation of the general features of the image shown in Plate 2. The strong coastal current north of Wainwright (km +750) and changes in course to avoid sea ice north of Point Barrow (km +900) led to fluctuations in streamer depth and consequent variations in the frequencies recorded. Use of a 75 m shot interval from km +0 to +145 and from km +735 to +980 provided an effective source energy in the resulting 27-fold stack trace that is about one-third less than that resulting from the 50-m-interval, 40-fold data acquired in most of the survey. Changes in seafloor geology from gassy unconsolidated sediments to exposed crystalline basement result in large changes in near-surface absorption of seismic energy, leading to abrupt changes in apparent lower-crustal reflectivity that presumably do not correspond to real changes in lower-crustal composition and structure. Examples can be seen near km –45 and km –175 in the seismic section in Plate 2.

Throughout this chapter, references are made to the (two-way) traveltime (in seconds) to reflections, and to the depth (in kilometers) of the corresponding reflector. These depths are obtained by multiplying one-half the (two-way) traveltime by the appropriate average seismic velocity. For shallow reflections (typically sedimentary reflections) we can directly measure the appropriate seismic velocity from the shape of the reflection traveltime curve (the normal-moveout curve) (e.g., Hatton et al., 1986; Yilmaz, 1987). For reflections deeper than the maximum source-receiver offset (4.2 km), such estimates of velocity become progressively more unreliable, and the appropriate seismic velocity is best estimated from nearby refraction surveys, such as those of Houtz et al. (1991), Cooper et al. (1987), and Wolf et al. (this volume). In the absence of nearby refraction profiles, averages from global compilations (e.g., Christensen and Mooney, 1995) provide a crude guide to the typical range of seismic velocity at different depths. Estimates of depth from reflection profiles unsupported by coincident refraction data have probable uncertainties ranging from a few percent within sedimentary basins to ±10% for crustal thickness.

DESCRIPTION OF DATA

All features described in this section are indicated in Plate 2 and may be located by their distance north (+km) or south (–km) of the Bering Strait. Plate 2 also shows shotpoint numbers along the profiles that may be tied to the shotpoint locations in Plate 1 of Miller et al. (this volume, Preface). Regional basins and structures are shown in Plate 1 of Grantz et al. and on the line drawing in Figure 2.

Northern region: Chukchi Shelf north of Herald Arch (Plate 2, panel A and right portion of panel B)

Beaufort rifted margin. The northern limit of our transcontinental transect is at 190 m water depth close to the modern

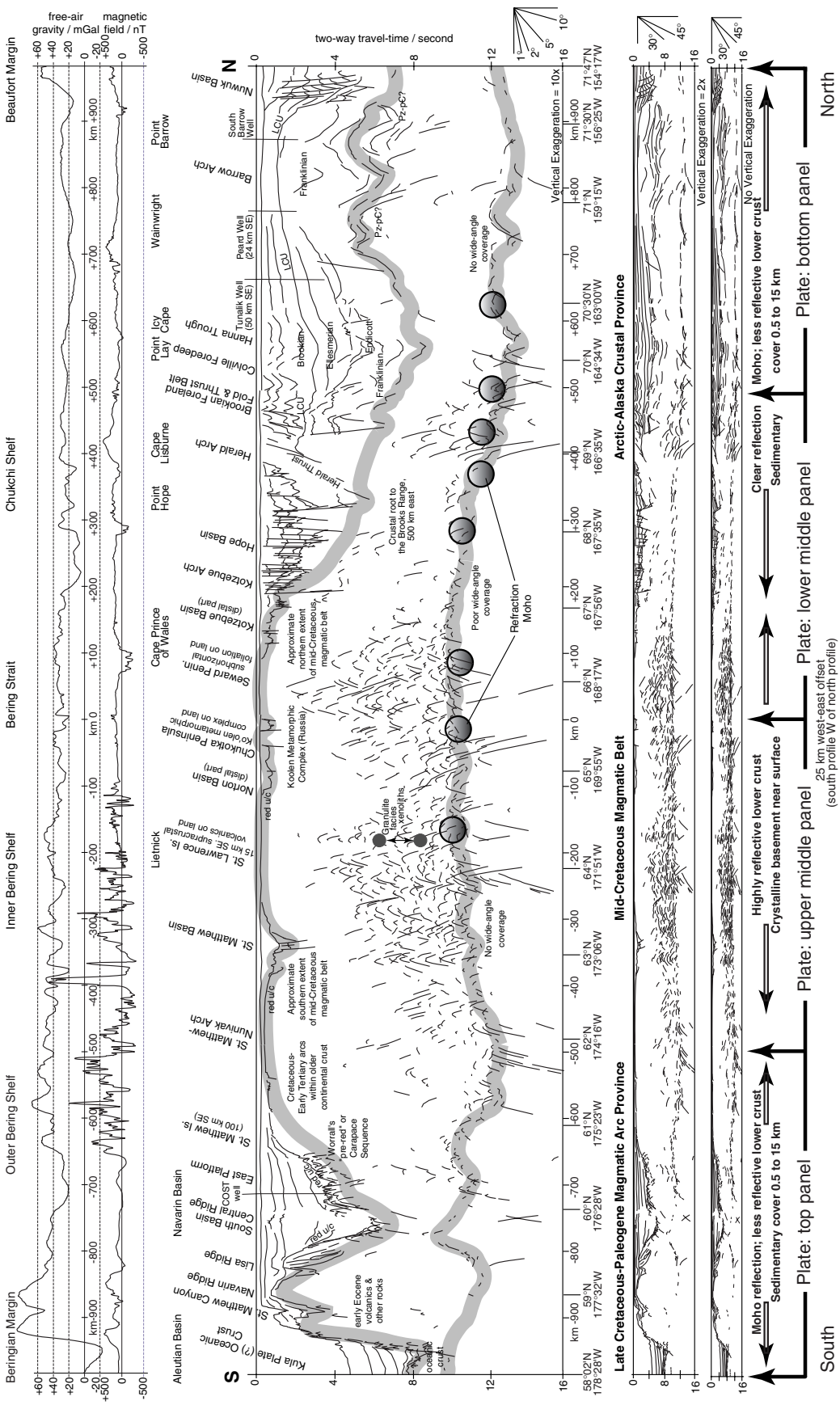

Figure 2. Summary line drawing of reflection transect from Beringian margin to Arctic margin (S–N in Fig. 1), crossing entire North American continent. Note that line drawing comprises south half of western transect merged at Bering Strait with north half of eastern transect (same data as shown in Plate 2). Bottom section is true scale for crustal velocity of 6 km/s; middle and upper sections are 2 and 10 times vertically exaggerated, respectively. Thick gray lines in upper panel: upper line is base of stratified sedimentary reflections (approximate base Franklinian below Chukchi Shelf and Beaufort margin; approximately middle Eocene [red unconformity] on Bering Shelf); lower line is reflection Moho estimated from our reflection transect (Plate 2). Small gray circles in center of upper panel indicate depth range of granulite xenoliths from Saint Lawrence Island (after Wirth et al., this volume; Miller et al., this volume, Chapter 10). Large circles in north half of upper panel are estimates of traveltime to refraction Moho (from Wolf et al., this volume). LCU is Lower Cretaceous unconformity; red u/c is Eocene red unconformity. Free-air gravity and magnetic profiles recorded along ship track, smoothed with ~1 km running filter, are shown at top of figure.

Beaufort shelf edge, and shows a progradational prism of sedimentary rocks composed of Cretaceous and Tertiary marine strata deformed by numerous listric normal faults. The listric faults have a predominantly northerly dip, and were presumably driven by gravitational body forces created by the free face of the adjacent continental slope. Tertiary strata extend to 2.5 s at the north end of our transect and overlie, in part unconformably, more-strongly rotated Cretaceous strata. The listric faults that rotate the Cretaceous strata sole into a listric normal fault of lower angle at the approximate position of the Lower Cretaceous unconformity (breakup unconformity) (see Fig. 2 and Plate 2) (Grantz et al., 1990), and extend upward through the Tertiary beds to within 0.1 s (~0.1 km) of the seafloor. The basal, low-angle, listric fault truncates synrift marine strata of Jurassic and early Early Cretaceous age that were deformed, in places intensely, by down-to-the-basin (north-dipping) listric faults (Grantz et al., 1990). These faults represent gravitationally driven failure of the northern margin of the rift shoulder during initial stages of opening of the Canada Basin.

The Lower Cretaceous unconformity becomes increasingly visible south of km +935, where it is at 3 s. A dramatic hinge line occurs at km +915 (Fig. 2), south of which Cretaceous normal faults are not present and the postrift succession thins gradually onto the Barrow Arch. The broad crest of this arch, in the vicinity of km +835, is a basement high of compound origin. Its structural morphology and relief were developed mainly during the Early or Middle Devonian, when Ordovician and Silurian strata of the Franklinian geosyncline were folded, mildly metamorphosed, and raised above sea level. Widespread erosion created a broad, southward-dipping Arctic platform (present coordinates) at the margin of the North American craton that was initially covered by nonmarine sediments at the base of the Devonian and Lower Mississippian Endicott Group. The structural elevation of the northern part of the Barrow Arch was augmented by uplift related to the Jurassic prerift extension and early Early Cretaceous seafloor spreading that created the Canada Basin. This uplift created a series of erosional unconformities along the crest and north flank of the Barrow Arch, culminating in the formation of the regionally significant Lower Cretaceous unconformity.

Franklinian strata (Ordovician and Silurian) and underlying Cambrian (?) and Precambrian bedded rocks. Although imaging is not optimal in this area (perhaps because of the strong coastal current and/or numerous course adjustments required to avoid sea ice north of the Barrow Arch), a thick reflective sequence is visible beneath the Lower Cretaceous unconformity, to 7 s and locally 8 s between the Cretaceous hinge line and at least as far south as km +630, near Icy Cape. Imaging of this sequence farther southwest, if it exists, is hampered by the overlying Brookian and Ellesmerian strata that thicken rapidly to the southwest. We follow Grantz et al. (1987) in interpreting this succession as Franklinian and underlying Cambrian (?) and Proterozoic sedimentary rocks. This may be the first time the full depth of the Cambrian and Proterozoic succession has been imaged here because typical industry data in this area are recorded to only 6 s. These deep reflections are not multiples of the overlying Ellesmerian and Brookian reflections (which extend to 4.5 s at km +630), because the reflections we interpret as Franklinian or older have stacking velocities of ~5 km/s and implied interval velocities (poorly determined because the far offset recorded was only 4.2 km) of >6 km/s at 7 s (consistent with Sherwood's [1992] velocities and interpretation of a deep Franklinian carbonate unit). Craig et al. (1985) interpreted our Franklinian and underlying Cambrian (?) and Proterozoic sedimentary rocks as a lower Ellesmerian clastic wedge, downdropped by 6 km to the west across the 200-km-long coast-parallel, northwest-dipping Barrow fault; and Sherwood (1992, his Fig. 3) reinterpreted the so-called Barrow fault as a steep (70°–80°) southeast-dipping thrust fault with 10 km of vertical throw. However, our transect shows no evidence for any major fault in the position suggested by Craig et al. (1985, their Fig. 7) at ~km +750 (Plate 2), and the gravity field over the North Slope and Chukchi Sea shows no evidence of the coast-parallel gradient that would be expected across such a major fault (e.g., Barnes et al., 1994; Klemperer et al., this volume, Chapter 19, their Fig. 3).

The depth, seismic character, and low dip of reflections from 9 s at km +555 to 6.5 s at km +465 beneath the Brookian fold belt suggest that the contact between the Franklinian sequence and underlying beds may underlie the entire Arctic Alaska Basin and Colville foredeep as far south as the Lisburne Peninsula. The sporadic occurrence of similar reflectors at depths of 4–6.5 s as far south as km +195 suggests, but more speculatively, that the contact may also underlie the Hope Basin at least as far south as the north flank of the Kotzebue Arch. Paleogeographic reconstructions (Plafker and Berg, 1994b) show the Franklinian and older sedimentary rocks located on the southern margin (in the modern coordinate system) of the Arctic Alaska microplate that continues in the subsurface south of the Brooks Range orogen (Fuis et al., 1995).

The northern extension (modern coordinates) of the Franklinian basin and underlying succession imaged on our transect should now be in the conjugate rifted margin of Arctic Canada (Rickwood, 1970; Embry, 1990; Grantz et al., 1998; Mickey et al., this volume), possibly in the region of Prince Patrick Island (Sherwood, 1992). The Franklinian strata on our transect are laterally equivalent to a belt of deep basin deposits, several thousand meters thick, consisting of lutite, turbidite, radiolarian chert, carbonate debris flows, and volcaniclastic rocks of Cambrian to Early Silurian age. These strata are between the lower Paleozoic carbonate shelf strata that underlie northern Greenland and the Canadian Arctic Islands on the southeast, and the Amerasia Basin margin on the northwest (Higgins et al., 1991; Trettin et al., 1991). Restoration of counterclockwise rotation opening of the Canada Basin would place these basin deposits of the Canadian Arctic Islands against the Ordovician and Lower Silurian argillite and graywacke sequence of the North Slope of Alaska and the Franklinian sequence of the Chukchi

Shelf (Grantz et al., 1998, their Fig. 6), which we interpret to be as thick as 14 km beneath the Barrow Arch. Closure of the Canada Basin would also place the high-velocity pre-Franklinian sedimentary strata and crustal basement imaged on our seismic profiles, together as thick as 25 km, against Proterozoic and older middle and lower continental crust beneath the Canadian Arctic Islands adjacent to the Amerasia Basin (Sweeney et al., 1986), which are 30–35 km thick. The thickness (to ~10 km) of the high-velocity pre-Franklinian strata imaged on our seismic profiles suggests that they may correlate with the thick, gently folded Late Proterozoic (Hadrynian) successions of the southwestern Canadian Arctic Islands (Stockwell et al., 1970). These deposits include the shallow-water carbonates, evaporates, and sandstones (including quartzites) of the gently folded, 4-km-thick Shaler Group on Victoria Island, and have been mapped in the subsurface of Melville Island as a Proterozoic basin from 5 s to 9 s traveltime (~10 km thick) (Kanasewich and Berkes, 1990). Similar thick sequences may extend 1000 km along the strike of the Proterozoic and Franklinian margin, if the reflective strata on our transect are also laterally equivalent to the 6–8 s of layered reflections described by Coflin et al. (1990) in the Mackenzie Delta region.

Ellesmerian strata (Upper Devonian to Jurassic). Brookian strata above the Lower Cretaceous unconformity overlie the Ellesmerian sequence south of the erosional wedge-out of the Ellesmerian strata near km +880 (Fig. 2; Plate 2). These Upper Devonian to Jurassic Ellesmerian strata thicken smoothly southward from the wedge-out on the Barrow Arch to ~2 s (~4 km) at km +625, off Icy Cape. South of km +625 a series of Upper Devonian-Carboniferous grabens is present in the lowest part of the Ellesmerian sequence (the Endicott Group). The deepest of these, which is in the axial region of the Hanna Trough (Grantz et al., 1987; Sherwood et al., this volume), is ~30 km wide and centered at km +560. The Ellesmerian sequence within this graben is 1.5 s (~3.5 km) thicker (base at ~6.5 s) than adjacent Ellesmerian outside the graben. South of the graben, the base of the Ellesmerian rises from 5 s to 4 s before another 30-km-wide graben is encountered, centered at km +435 just north of Cape Lisburne. The presumed fault-plane reflections bounding this graben have true dips of ~45° (based on manual migration), and are reflective from 2.5 s at the Lower Cretaceous unconformity, which is offset ~0.2 s (~0.1 km) across at least the southern of these faults, to perhaps 7.5 s (possibly base of Franklinian). (Note that in Plate 2 interpreted faults are shown in their true structural positions [normally much steeper than the unmigrated reflections because the faults are typically steep], in contrast to the sedimentary reflections, which are marked in their unmigrated positions [normally close to the correct location because they typically dip at shallow angles].) Resolution of the Ellesmerian strata is lost immediately north of the Herald Arch (km +390), offshore Cape Lisburne, and their extent farther south is speculative.

Brookian strata (Cretaceous and Tertiary). The Colville foredeep contains clastic sedimentary rocks eroded from the area now covered by the Hope Basin, as well as the Brookian orogen to the south (Moore et al., 1994). The maximum thickness of strata in the Colville foredeep along our transect is 3.1 s (nearly 5 km), attained close to the axis of the underlying Hanna Trough. However, the general lack of faulting of the Lower Cretaceous unconformity (Fig. 2; Plate 2) suggests that the foredeep resulted from sedimentary loading rather than the reactivation of older extensional structures in the region of the Hanna Trough. The southern part of the Colville Basin is deformed in the distal Brooks Range fold and thrust belt, which is the result of deformation above the Late Cretaceous or Paleocene Herald thrust, which follows the Lower Cretaceous unconformity north of Cape Lisburne. At the deepest part of the basin (near the Hanna Trough), the Brookian foreland folds have wavelengths of ~30 km and amplitudes of ~0.3 s (~0.35 km), the amplitudes diminishing northward. At the south margin of the Colville Basin, just north of Cape Lisburne, fold wavelengths on the seismic section (Plate 2) are as short as ~15 km, fold amplitudes exceed 1 s (~1.5 km), and the folds are broken by blind thrusts. Imaging of the Brookian sedimentary rocks deteriorates to the south as fold limbs steepen, and all resolution is lost at Cape Lisburne where the thrust folds are replaced by imbricate thrust splays that bound horsts of Ellesmerian as well as Brookian strata at the Herald Arch (Plate 2) (Grantz et al., 1970).

Crystalline basement and Moho. Few intracrystalline basement reflections are visible on our transect north of the Herald Arch, yet the reflection Moho is visible almost ubiquitously from the arch at km +400 to the Cretaceous hinge line at km +915. Across this 500-km-wide region the Moho reflection is a characteristic single bright reflection separating nearly reflection-free lower crust from reflection-free upper mantle. The reflection Moho varies between 12 s and 13.5 s over this distance, more due to velocity pushdown than to laterally changing velocities in the crystalline basement. Beneath the thicker part of the Colville Basin section, from km +650 to +420, the traveltime to reflection Moho varies directly with the thickness of the basin, showing that the basin passively loaded and depressed the crust without corresponding basement deformation. For example, the Lower Cretaceous unconformity deepens from 2 s at km +645 to 3 s at km +565, an increase in depth of ~0.8 km across 80 km. Across the same distance the reflection Moho is also delayed by the same traveltime, deepening from 12 s to 13 s. We speculate that beneath the Barrow Arch changes in traveltime to reflection Moho may similarly represent changes in thickness in the overlying Franklinian and Proterozoic basins. The Moho traveltime varies from 13.5 s (km +710) to 12.5 s (km +755) to 13.5 s (km +810) across this area, seeming to correlate with the long-wavelength warping of the Franklinian and pre-Franklinian sedimentary reflections at 6–7 s.

The subsedimentary crystalline basement across the 500-km-wide region from the Cretaceous hinge line to the Herald Arch is <20 km thick, in places <15 km thick, suggesting that in Late Proterozoic and early Phanerozoic time this part of the Arctic Alaska plate must have been a very broad, highly extended,

continental margin (less than half average continental crust thickness). True depth to Moho probably varies from ~39 km beneath the Barrow Arch to ~35 km beneath the axis of the Hanna Trough (depth calculated using sedimentary rock velocities from our reflection data, and crystalline-basement velocities of 6.5 km/s). Wolf et al. (this volume) use wide-angle data to determine a Moho depth of 35 km and traveltime of ~12 s beneath Point Lay, in good agreement with our reflection Moho (Fig. 2), thereby encouraging the conventional assumption that the reflection Moho and refraction Moho are equivalent (Klemperer et al., 1986; Mooney and Brocher, 1987) beneath the Chukchi Shelf.

Northern region: Herald Arch and Hope Basin (Plate 2, central portion of panel B)

Herald fault zone and arch. The Herald fault zone and arch is the northwest-southeast–trending belt of nonreflective acoustic basement at the seafloor (Grantz et al., 1987) that emerges onshore as the Tigara uplift of Ellesmerian and Franklinian strata exposed in east-vergent thrust sheets on the Lisburne Peninsula (Moore et al., 1994, and this volume) (Plate 2). These thrusts are Late Cretaceous to Paleocene in age, because they deform Albian and probably Cenomanian strata (Campbell, 1967), but do not deform or tilt Eocene and younger Hope Basin sedimentary rocks (Tolson, 1987a; see following section). Late Early Cretaceous apatite fission-track cooling ages (ca. 115 Ma) (Moore et al., this volume) date the event that caused imbricate thrusting in the Lisburne Peninsula. Because the Brookian structures are subparallel to the Herald Arch in the offshore region, it is difficult to distinguish the two in our regional deep profile. However, we may take the north limit of the Herald Arch as the ~20° south-dipping reflections that project to the surface at km +410 and reach the prominent Lower Cretaceous unconformity reflection (Brookian detachment) at ~2 s, where the Lower Cretaceous unconformity changes from horizontal to the north to ~10° south-dipping to the south. Scattered south-dipping reflections extend at least 40 km to the south beneath the Hope Basin, as far as km +370. In addition, south-dipping reflections at least as deep as 8 s between km +340 and km +325 may represent Franklinian or older strata rotated by either north-dipping normal faults of the Hope Basin or possibly the south-dipping extension of the Herald thrust. However, clear evidence for the Herald thrust is only visible to 3 s traveltime, and it cannot be reliably traced south of the northern onlap of the Hope Basin at km +380.

Hope Basin. Our transect crosses the Tertiary Hope Basin from the Herald Arch at km +380 to the Kotzebue Arch at km +185 (Tolson, 1987a). Along our transect the dominant structural style controlling the basin is high-angle normal faulting, the two deepest points reaching 3.6 s (~6 km) in half-grabens within the basin at km +275 and at km +315. The beds in these half-grabens were downdropped by 2 s (~3 km) from a central horst that is between km +285 and +305, just southwest of Point Hope. The northern half-graben is bounded and underlain by prominent fault-plane reflections that can be traced to >6 s at km +330. The listric appearance (decrease in dip to the north) of the fault-plane reflections in this unmigrated section may be an imaging artifact (pull-up) due to the decreasing sedimentary thickness to the north that bends the reflection from a fault that is in reality planar (cf. Peddy et al., 1986). Both half-grabens are underlain by low-frequency reflections (at 5–7 s at km +265 to +275; at 4–6 s at km +315 to +335) that also dip inward toward the central horst. These may therefore be Paleozoic strata that were also rotated by the Hope Basin faults. Similar reflections are seen at 4–5 s, km +200, and at 3–4 s, km +170. North of km +315, the Hope Basin sedimentary sequence thins northward to the Herald Arch across several south-dipping normal faults (antithetic to the main fault). South of km +275 the basin gradually thins southward toward the Kotzebue Arch across many south- and north-dipping faults.

The oldest rocks in the Hope Basin are middle Eocene (pre-41 Ma) sedimentary rocks that, based on the section penetrated in two coastal wells at the eastern end of the Kotzebue Basin (Fig. 1), unconformably overlie crystalline limestone, phyllite, and dolostone of Paleozoic (?) age (Tolson, 1987a; Plate 1). The stratigraphy of the Cape Espenberg No. 1 and the Point Nimiuk No. 1 wells in the eastern part of the Hope Basin (CE and PN in Fig. 1) is summarized in Plate 1. In the Tertiary section, Tolson (1987a) defined a nonmarine and deltaic seismic-stratigraphic Unit I of Eocene and Oligocene age, a generally nonmarine lower Miocene Unit II, and a generally marine middle Miocene to Pleistocene Unit III. Tolson's (1987a) seismic stratigraphy is particularly clear at km +275, where Units I, II, and III are separated by more strongly reflective bands at 1.3 and 2.3 s. Unit I is only present in the deepest half-grabens, which appear to be bounded by growth faults initiated at the earliest stage of basin formation. Unit II (clearly visible between km +280 and the Kotzebue Arch) has a comparatively uniform thickness (~0.8 s), suggesting a broader pattern of thermal subsidence. Unit III reaches a thickness of 1.8 s (~1.8 km) at km +215, is offset by many high-angle normal faults that reach essentially to the seafloor, and thins to 0.5 s over the Kotzebue Arch.

Tolson (1987a) suggests, from indications that some of the faults bifurcate upward into flower structures, that the first phase of deformation in the Hope Basin was Eocene transtension on a dextral-slip fault system. This extension in the Hope Basin possibly accommodated dextral slip along the Kobuk fault system (e.g., Kirschner, 1994; Moore et al., 1994). The 100 km gap between onshore basement exposures that define the Kobuk fault system and Tolson's offshore seismic data precludes a more certain statement. (Crustal thinning arguably related to this transtension is discussed in the following section.) The second phase of deformation in the Hope Basin was a middle to late Miocene reinitiation of extension on both reactivated and newly formed normal faults. Extension continues to the present, indicated by the diffuse belt of seismicity with both extensional and dextral strike-slip focal mechanisms, the Bering rift zone of

Mackey et al. (1997) that extends across the southern Hope Basin. Just as the modern faulting is presumed to represent a far-field effect of shortening in southern Alaska and concomitant extrusion of western Alaska (Mackey et al., 1997), so the Eocene faulting possibly represented a far-field accommodation of changing boundary conditions imposed on the North American plate by Pacific subduction.

Crystalline basement and Moho. Deep-crustal reflectivity is fairly pronounced between 10 and 12 s below the southernmost Colville Basin and Herald Arch (km +440 to +385), and scattered reflectivity is also visible in the middle crust in this area. Beneath the southern part of the Herald Arch and the entire Hope Basin, imaging of the deep crust is poor, with only a faint reflection Moho, and few scattered reflections. One might speculate that the bright reflectivity near km +400 represents an imaging window through shallow high-velocity rocks into the lower crust that typifies a much broader region. However, it is not obvious that imaging should be dramatically clearer through the 2 s (~3 km) Brookian section at km +400 than through the 1 s (~1 km) Neogene section at the northern and southern margins of the Hope Basin at km +370 and +185, or through the <1 s Brookian section over the Barrow Arch north of km +800. Because the few scattered lower-crustal reflectors observed beneath the Hope Basin are dipping and of lower amplitude than the flat Moho reflection (in contrast to the character imaged in the central region of our transect), we argue that the lower crust is similar beneath the Barrow Arch, Colville foredeep, and Hope Basin, and that these are all parts of the autochthonous Arctic Alaska plate. The brighter reflectivity around km +400 is presumed to be a local feature.

The reflection Moho, which can be traced with only minor difficulty beneath the Hope Basin, rises from 12 s beneath the Herald Arch (km +400) to 10.5 s below the northern major half-graben of the Hope Basin (km +320), and remains fairly uniformly at this level to the Kotzebue Arch. Because Cenozoic sedimentary thickness increases from 0 to 3 s (~5 km) over this distance, the apparent shallowing of reflection Moho across the Hope Basin represents a true thinning of the pre-Tertiary crust of as much as ~10 km. This thinning implies up to ~30% extension during formation of the Hope Basin, assuming that the pre-extensional crust was of uniform thickness. However, because we infer that there was preexisting topography (to provide a western source for the mid-Cretaceous Corwin Delta; summarized in Moore et al., 1994) and hence a crustal root, more than 30% extension is locally required beneath the deepest grabens of the Hope Basin. Typical extension may have been only 20%–25% if an average sedimentary thickness of 2–3 km, and traveltime to reflection Moho of 10.5 s, is taken for the entire basin. Although the crustal refraction model of Wolf et al. (this volume) shows essentially no thinning of the crust from Cape Lisburne to the Bering Strait, their model is not inconsistent with the thinning claimed here because their recording seismographs were all located outside the Hope Basin (Fig. 1). Traveltime delays from seismic source points along the ship track above the Hope Basin depocenter are increased because of near-surface sedimentary rocks; however, only shots with a source-receiver midpoint close to the depocenter can image the crustal thinning. Because of the onshore-offshore recording geometry, only shots more than ~200 km north of Cape Prince of Wales and more than ~200 km south of Cape Lisburne have midpoints over the Hope Basin depocenter. At these long offsets the seismic arrivals were too weak to be reliably observed and so were not used in the modeling presented by Wolf et al. (this volume). The Wolf et al. model is, however, an appropriate measure of crustal thickness, 32–34 km, north and south of the Hope Basin.

The western projection of the Kobuk fault (Patton et al., 1994) strikes toward a zone of antithetic normal faults along the north flank of the Kotzebue Arch that has far more structural relief than the south side of the Kotzebue Arch, and that forms the south side of the Hope Basin (Fig. 1; Plate 1). This geometry suggests that the westward-diverging normal faults of the Hope Basin may represent a transtensional system at the trailing edge of the Brooks Range block that created the Hope Basin as it moved eastward along the dextral Kobuk fault (Tolson, 1987a; Kirschner, 1994) during the Paleocene or early Eocene. Based on seismic mapping of the Hope Basin in United States waters (Tolson, 1987a; Kirschner, 1988) and Russian waters to 172°W (Eittreim et al., 1978), and on the Bouguer gravity anomaly of −10 to −20 mGal (Ostenso, 1968; see also Klemperer et al., this volume, Chapter 19, their Fig. 3), the Hope Basin continues for ~400 km in a west-northwest direction, and so could conceivably have accommodated 80–100 km dextral motion on the Kobuk fault system. Knowledge of the displacement history of the western end of the Kobuk fault remains poor, but W.W. Patton Jr. (2001, personal commun.) reported that Upper Cretaceous paralic deposits containing 80 Ma volcanic ash appear to have been offset dextrally a minimum of 40 km along the lower reaches of the Kobuk River near 160°–161°W. It is therefore possible that dextral displacement along the Kobuk fault created the transtensional faults that opened the Hope Basin, but specific correlation of these events is not yet established. In contrast, some terrane reconstructions suggest sinistral motion along the northeast flank of the nascent Hope Basin and the Kugruk fault zone (which separates the Seward Peninsula from the Yukon-Koyukuk Basin) in order to relocate the Seward Peninsula southward to its present location (Plafker and Berg, 1994b).

Central region: Bering Strait, Saint Lawrence Island, and Inner Bering Shelf (Plate 2, left of panel B and panel C)

Kotzebue Basin. The Kotzebue Basin (Plate 2) is little more than a shelf, locally with a broad, rather shallow sag, between the crest of the asymmetrical Kotzebue Arch and the Seward Peninsula. The Kotzebue Basin may be regarded as a southern extension of the Hope Basin; Unit II and some Unit III Neogene sedimentary rocks (Tolson, 1987a) are present for 100 km along our transect from the Kotzebue Arch at km +185 to the southern wedge out of Hope Basin fill against basement of the Seward

Peninsula at km +85. It is distinguished from the main Hope Basin by the near absence of normal faulting, and by the much smaller sediment thickness. The maximum thickness of the section along our transect is 1.4 s, ~1.5 km, from km +160 to +175, and it is never more than 0.8 s thick south of km +150.

Norton Basin. The transect of Figure 2 and Plate 2 is offset discontinuously 25 km to the west at km 0 in the Bering Strait, and misses all but the most distal part of the Norton Basin. Norton Basin has a stratigraphy that is similar to that of the Hope Basin where drilled at ~166° and 164°W (~4 km of Eocene to Pleistocene strata), but may have a latest Cretaceous-Paleocene early history represented by an additional 2 km of strata below the deepest drilled horizon (Marlow et al., 1987; Worrall, 1991). The stratigraphy of the Norton Sound COST No. 1 and No. 2 wells in the eastern part of the basin (No1 and No2 in Fig. 1) is summarized on Plate 1. Unlike in the Hope Basin, a regional unconformity is present within the Eocene section above folded early basin strata (carapace sequence of Worrall, 1991). This unconformity is widely mapped as the broadly contemporaneous, ca. 43 Ma "red" event across all basins of the Bering Shelf (Worrall, 1991), and could be equivalent to the pre-41 Ma unconformity of the oldest Hope Basin sediment onto basement. The Norton Basin has the same spatial relation to the Kaltag fault (northwest of the possible terminus of a regional dextral fault) that the Hope Basin has in relation to the Kobuk fault system, suggesting that the Norton Basin formed by distributed transtensional faulting at the trailing edge of the north block of the dextral Kaltag fault (Fisher et al., 1982; Worrall, 1991; Kirschner, 1994). The Norton Basin could thereby allow the Kaltag fault to terminate on the shelf at this system of basins (e.g., Worrall, 1991), or could alternatively transmit the Kaltag strike-slip motion to the shelf edge or plate boundary.

At km –15 (negative distances are south of Bering Strait) small normal faults allow accumulation of 0.8 s (~0.7 km) of Tertiary sediments in a basin 20 km wide where crossed by the transect. The western feather edge of the Norton Basin is visible from km –45 to –125, reaching maximum thickness on our transect of 0.7 s at km –85.

Saint Matthew Basin. The Saint Matthew–Hall Basin has attracted only scant attention in the published literature (Marlow et al., 1976), presumably because it is both remote and does not have sufficient thickness to produce hydrocarbons. For the Saint Matthew–Hall Basin, unlike other basins on the Bering Shelf, our seismic data provide a significant update of previous mapping, which suggested that it was only ~1 km deep west of Saint Lawrence Island (Kirschner, 1988; Worrall, 1991). On our seismic profile, an almost unfaulted thermal subsidence or sag phase from km –305 to km –415 reaches a maximum thickness of 1.1 s (~1 km) at km –350, and overlies two prominent tilted fault blocks in which sedimentary reflections continue to 2 s (~3 km total depth) at km –345 and km –355. By analogy with the Norton Basin and the Navarin Basin, we regard the tilted rift-phase sedimentary rocks as largely "pre-red unconformity" (Fig. 2) (Worrall, 1991; see also following Navarin Basin discussion). Another, much smaller, trough of strata pre-red unconformity may be present at km –385, to 1.2 s.

Although our single profile precludes any firm conclusions about the areal extent of the Saint Matthew Basin, the existence of a continuous basin from the Alaskan coast to southwest of Saint Lawrence Island may suggest that the strike-slip systems believed responsible for aspects of the development of the Hope and Norton Basins may also have extended across the shelf beyond Saint Lawrence Island (Holmes and Creager, 1981; Scholl et al., 1970).

Crystalline upper crust of Bering Strait and Saint Lawrence. The Bering Strait region and the Inner Bering Shelf are characterized by broad basement arches with intervening sedimentary basins. So-called acoustic basement (labeled as such only by the absence of well-defined reflections) is at or very close to the seafloor along our transect between the Kotzebue Basin and the Norton Basin, km +85 to km –5; between the western distal onlaps of the Norton Basin from km –25 to km –45; and between the Norton Basin and the Saint Matthew Basin from km –125 to km –305. As with many, if not most, crustal-scale reflection profiles, the uppermost crystalline crust returns few laterally coherent reflections, in part due to technical reasons. These include higher-amplitude source-generated noise (refracted and reflected reverberations or multiples) and greater sensitivity to correct stacking velocity and lower stacking fold than at longer traveltimes; and coarse shot spacing and low frequencies, chosen to allow deep-crustal recording, that are inappropriate to image complex, nonstratified near-surface geology. It is therefore no surprise that we cannot attribute any specific reflections to specific rock bodies, e.g., plutons or metamorphic complexes. It is noteworthy, however, that close to the Seward Peninsula we record coherent reflections within the upper 5–10 km of crust that offer at least the prospect of mapping structural fabrics. Close to where our reflection profile passes only 10 km from Cape Prince of Wales, from km +55 to km +40, reflections from 1 s to 3 s (~3–9 km) rise to the south at ~45° (after hand migration), projecting to the surface at ~km 35; and from km +35 to km 0 reflections from 1.5 s to 3 s form an antiform with flanks dipping ~20°. As with any individual seismic line, we can only assume that our reflection line is a true dip line recording in-plane reflections. Possibly correlative reflections on profile 3B, 25 km due west, are no shallower than 3 s, suggesting that this antiform plunges 10° west. Even though these reflectors are relatively close to land, it is unclear to what they are related. Some of the reflections could represent the Cretaceous granites that underlie the region (exposed on the Diomede Islands 30 km to the west [Shumway et al., 1964] and on the Seward Peninsula [e.g., the Kigluaik pluton, Amato et al., this volume]), although these granites are typically undeformed, so reflectivity would likely represent internal compositional variability (e.g., Amato and Wright, 1997). Alternatively, and we believe more likely, the reflections might represent undulatory domal structures and shallow-dipping foliations in the low-grade metasedimentary rocks exposed 30 km to the east in the Seward

Peninsula (Amato et al., this volume). A 30-km-long industry reflection profile 30 km east of km +65 to +35, recorded to 6 s traveltime (Fig. 1; Tolson, 1987b, p. 131), shows a reflection dipping 10°N from 2.5 to 4.5 s. Tolson (1987b) suggested that this reflector corresponds to a low-angle detachment at the top of a metamorphic core complex represented by blueschist outcrops in Seward Peninsula. Our data cannot corroborate Tolson's interpretation and suggest, at the least, that the crust exhibits more complexity than a single domal structure.

The only other subsedimentary reflections on this part of the transect shallower than 3 s that are demonstrably not multiples are at km –185 and km –235 to km –260 at ~2.5 s just north of Saint Lawrence Island. These reflections may be described as the shallowest manifestation of what we loosely term lower crustal reflectivity, in that these horizontal to subhorizontal reflections continue downward to the base of the crust.

Crystalline basement, Moho, and intramantle reflectors. A gradual but significant change in the character of lower-crustal reflections and the reflection Moho occurs south of the Kotzebue Arch. Unlike the northern segment in which the reflection Moho stands out as brighter than the scattered lower-crustal reflections, across this central segment the reflection Moho is normally identified as the base of a sequence of many reflections occupying the lower one-third to two-thirds of the crust, and marking the transition to a usually nonreflective upper mantle. This layered character of the lower crust is most clearly seen in the center of our central segment, beneath the Bering Strait and near Saint Lawrence Island, and disappears southward near the Saint Matthew–Nunivak arch. Although the changes in crustal character are gradual, and consideration must be given to the effects of weather on the quality of imaging along this profile (see previous section on acquisition, processing, and interpretation of seismic data), we believe, on the basis of our two parallel profiles, that this reflective, layered lower crust distinguishes the crust beneath the central segment of our transect from less-reflective regions to the north and to the south.

Flat-lying or very gently dipping reflections, sometimes called laminated lower crust (e.g., Meissner, 1986), occupy a 500-km-long sector of the deep crust, from the southern half of the Kotzebue Basin (km +120) to the southern half of the Saint Matthew Basin (km –380). In some places the middle crust exhibits more steeply dipping reflections above the deeper crustal flat-lying reflections, as from km +50 to km 0 in the Bering Strait. In other places the middle crust is apparently nonreflective above the deepest crustal flat-lying reflections, as at km –300 to –350 north of the Saint Matthew Basin. Elsewhere, the subhorizontal laminated crustal reflectivity occupies 6–7 s (~18 to 23 km) above the Moho, e.g., around km –40, km –180, and km –250. Lower crustal reflectivity commonly occurs at shallower depths beneath basement highs, partly due to clearer imaging where attenuating sediment is absent (e.g., the vertical panel of clearer imaging from km –35 to –45 directly beneath a clearly marked change in seafloor characteristics). Although it is impossible to prove in any specific location, we believe it likely that many of these regions of shallower lower crustal reflectivity mark real lateral changes in the rock fabric, e.g., perhaps from nonfoliated igneous bodies to gneisses. The substantial lateral changes in thickness of the laminated lower crust make it impossible to assign this reflective character to a single velocity layer in the model of Wolf et al. (this volume). Wolf's deepest crustal layer, ~8 km thick with velocity of 6.5– 6.7 km/s, represents the deepest 2 s of traveltime of the crust, which in a general way corresponds to the brightest reflectivity. However, in Wolf's model no distinction occurs between the velocity of the lower crust we identify as laminated, and the lower crust farther north we identify as lacking lower-crustal reflectivity. This observation helps refine our interpretation of the reflectivity as representing extensional tectonic fabrics with only a modest proportion of intruded mafic material.

From the southern half of the Kotzebue Basin (km +140) to the north flank of the Saint Matthew Basin (km –330), the deepest Tertiary sedimentary rocks are consistently above 1 s traveltime and the reflection Moho is everywhere between 10 and 11 s traveltime. Although neither our study nor that of Wolf et al. (this volume) would be sensitive to short-distance, large-magnitude changes in crustal velocity, our observations of reflection Moho are consistent with those of Wolf et al. that the crust is a uniform 32 km thick across this large region. Here the near-vertical reflection and wide-angle reflection results are in good agreement, unlike in the Hope Basin, because the wide-angle and near-vertical reflection points are nearly coincident, and because no major lateral variations in sediment thickness occur between the source and the receivers.

Globally, intramantle reflections are the exception rather than the norm on deep reflection profiles, with some spectacular exceptions (e.g., Warner et al., 1996; Cook et al., 1999). On Plate 2 most of the steep reflected phases visible below the reflection Moho are diffractions from intracrustal discontinuities, and appropriate migration would move them into the crust. Because our profiles are only recorded to ~17 s traveltime, we cannot recognize steep reflectors from within the mantle, and on these data, only reflections that continue substantially below the Moho with a gentle dip can truly represent intramantle structures. Even these reflections could be returning from steeper crustal structures obliquely crossing the transect. Assuming the reflectors are in plane, we identify three possible intramantle structures in the central segment of our transect. A single reflector is visible offshore Saint Lawrence Island, dipping south from 11.5 s (just below the Moho) at km –230 to 17 s (maximum traveltime recorded) at km –275. The true dip after (manual) two-dimensional migration at mantle velocities is ~20°, extending from 10.5 s to 16 s. Just south and just north of the Bering Strait, reflections dip north from 10.5 s at ~km +20 to 17 s at ~km +50; and from ~11 s at km –70 to 17 s at ~km –35. The true dips after two-dimensional migration at mantle velocities (8 km/s) are ~40°, and the true imaged extent is only to 13.5 s, so that only a small degree of obliquity of the reflector to the profile direction would mean that these reflections originated within the crust. We

cannot attribute the mantle reflectors to any specific tectonic episode, but elsewhere such mantle reflectors frequently have an association either with fossil subduction zones (e.g., Warner et al., 1996), or putative extensional shear zones in continental rifts (e.g., Klemperer and Hurich, 1990).

Southern region: Outer Bering Shelf, Saint Matthew–Nunivak Arch to Beringian margin (Plate 1, panel D)

Saint Matthew–Nunivak Arch. Below a thin veneer of Neogene sedimentary rocks (increasing from 0.4 s on the crest of the Saint Matthew–Nunivak Arch at km –450 to 0.7 s at the edge of the Navarin Basin at km –635), and the barest hints of an older stratigraphy (e.g., south-dipping reflections from 0.5 s to 1.0 s from km –540 to –550; a possible synformal sag from 0.6 s to 1.2 s between km –600 and km –615), the upper crust in this region is featureless (see Plate 2, panel D). Our upper-crustal image does not distinguish between different possibilities such as a transparent magmatic arc and an accreted terrane lacking a coherent stratigraphy.

Navarin Basin. The Navarin Basin is known from extensive industry seismic data, and so here we describe our reflection data based on the thorough interpretation of these data published by Worrall (1991) without adding significant new results. There is one industry exploration well in the basin (COST No. 1; Na1 in Fig. 1) for which depths to lithostratigraphic horizons have been tied via a sonic log and synthetic seismogram to intersecting seismic data (Turner et al., 1984, 1985; stratigraphy summarized in Plate 1). COST No. 1, crossed by our transect at km –715, passed through a minor late Miocene unconformity at 1.3 s (~1.1 km depth) visible as a basinwide bright reflection on our transect (Fig. 3) (blue reflection of Worrall, 1991), and reached the important late–middle Eocene unconformity (Figs. 2 and 3) (red unconformity of Worrall, 1991) at 3.3 s (3.9 km) (Turner et al., 1985). The angular relationships of these unconformities are better seen on data displayed with large vertical exaggeration (Fig. 3). The COST well penetrated an additional 1 km of "carapace sequence" (Worrall, 1991) nonmarine strata of Late Cretaceous age, including gas-bearing coal units that predate the red unconformity. The sequence is intruded by basaltic sills that yield Oligocene and Miocene ages (although these K-Ar whole-rock ages should be regarded as minimum ages; Turner et al., 1984; Marlow et al., 1987). The brightest reflections on our profile beneath 3.4 s (~4.2 km) are from below the top of the Cretaceous sequence and are likely from these sills or from the gas-bearing coals. Structural relations on industry seismic data, and dredge data from the Beringian margin, imply that the carapace sequence encompasses Upper Cretaceous to middle Eocene strata (Worrall, 1991), corresponding largely to the period during which the Beringian margin was an active transpressional plate boundary. The uplift and subaerial erosion that produced the red unconformity, and the immediately following rapid subsidence to deposit upper-bathyal middle Eocene strata ca. 42 Ma, are not obviously related to the tectonic abandonment of the Beringian margin as a plate boundary in the early Eocene ca. 56 Ma (Worrall, 1991).

Our profile bypasses the northern depocenter of the Navarin Basin (Fig. 1) and crosses the East Platform drilled by the COST well (the red unconformity is at 3–3.5 s, 3.5–4.5 km depth, from km –685 to –740); traverses the Central Ridge (km –750 to –755) into the South Basin (maximum traveltime to red unconformity is 6.3 s [~8.2 km] at km –770); then climbs out of the Navarin Basin across the Lisa Ridge (km –825 to –835; blue horizon unconformably overlies pre-red strata at 1.3 s, 1.1 km depth) and onto the Navarin Ridge (km –870 to –880; blue horizon directly overlies strata that predate the red unconformity at 0.7 s, 0.5 km; Fig. 3) (all terminology is after Worrall, 1991).

The sequence that postdates the red unconformity is remarkably unfaulted across the entire basin, with the notable exception of the Central Ridge (km –750 to –755), a nonreflective zone on our data. Worrall (1991) showed it as a flower structure that he inferred from prebasin structures to have been formed by a dextral strike-slip fault (his cross section A–A′ is subparallel to our section, and ~10 km to the southeast). Although we do not image faults within the Central Ridge, our profile clearly shows minor inversion of the Miocene sequence south of the Central Ridge: the pre–late Miocene sequence (1.5–2 s at km –775) thickens basinward to the north, but its upper boundary now dips south (Fig. 3). The strata that predate the red unconformity, or carapace strata, are poorly imaged on our profile, as on many industry profiles (but see Worrall, 1991, his Figs. 45–51), and their base is nowhere clearly defined. However, at least 1 s of reflections is recorded from 4 to 5 s at km –740, and at least 2 s from 2.5 to 4.5 s at km –810. Below the carapace sequence we may guess at the presence of a Lower Cretaceous and Jurassic subduction complex similar to that exposed on Cape Navarin (Worrall, 1991), but we lack any direct evidence, and the structural fabric predating the carapace strata has not been imaged on our or on industry profiles. Unlike the strata postdating the red unconformity, the sequence predating the unconformity is broadly deformed. What resemble normal faults on our data (e.g., just north of the Central Ridge where the pre-red sequence is apparently downdropped 1 s [~1 km] across a north-dipping fault at km –745), and small structures that produce a crosscutting diffractive appearance on our unmigrated profiles (e.g., on the East Platform from km –705 to –735), are interpreted on a dense grid of migrated industry data to be east-west–trending folds rather than faults (Worrall, 1991). Only on the north margin of the basin (km –670) and on the south flank of the Lisa Ridge (km –835) did Worrall (1991) interpret north-south–trending normal faults, downdropped to the east, and active contemporaneously with the orthogonal folds as expected from dextral shearing in a northwest-southeast direction.

Navarin Ridge, Beringian margin, Aleutian Basin. Late Miocene and younger strata overtop the carapace strata and underlying basement of Navarin Ridge (km –870 to –880), which separates the Navarin Basin from the sedimentary prism beneath the slope and rise of the Beringian margin. The modern shelf

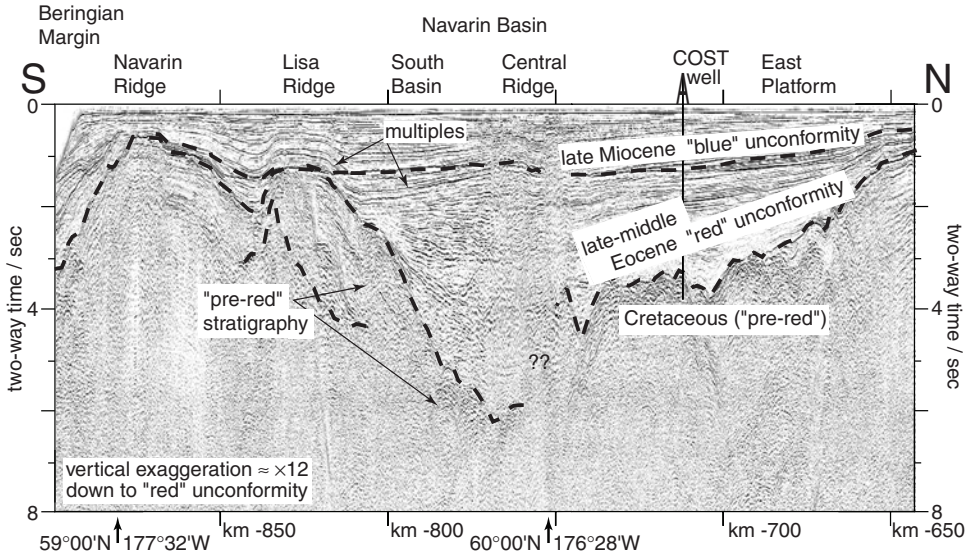

Figure 3. Seismic section across Navarin Basin. Acquisition and processing details as for Plate 2, except that data are horizontally compressed by factor of 5 with respect to Plate 2. Vertical exaggeration is ~12× for sedimentary rocks with velocity of 2.5 km/s (approximate average velocity down to red unconformity).

edge at km –895 has prograded only 15 km beyond the late Eocene shelf edge on the eroded flank of the Navarin Ridge. The slope is dissected by canyons (km –895 to –905), some of exceptional size, that produce rough seafloor topography crossed obliquely by our transect, and that cut back into the shelf eroding through the Tertiary strata into the pre-red unconformity or carapace sequence. The mean slope is about 3°, from 0.2 km water depth at the shelf edge to 3.2 km depth at km –945. The red unconformity emerges at the seafloor at ~km –935, so that pre-red strata crop out on the lower slope below ~2.8 s (2.1 km water depth). Carapace rocks including Cretaceous limestones and siltstone, and early Eocene arc volcanic rocks, have been dredged in this position (Jones et al., 1981; Davis et al., 1989). No structure is visible within the pre-red unconformity complex, here presumed to include a pre–late Eocene accretionary complex, although rock dredging has not recovered any such samples (Jones et al., 1981). At the foot of the slope the supposed accretionary complex is onlapped by oceanward-thickening terrigenous and hemipelagic sediments of the Aleutian Basin that postdate the demise of the active margin (Worrall, 1991). This presumably early Eocene to Holocene basin reaches 2 km thickness at the south end of our profile. Beneath a reflection at 6.4 s at km –980, sedimentary strata thicken toward the margin and contribute to the supposed accretionary prism, and thus presumably date from the period of active oblique subduction (pre-56 Ma), during and before the early Eocene. The diffractive horizon from 7.8 s at km –980 to 8.6 s at km –950 marks the top of oceanic crust basalts ascribed to the Kula plate by Scholl et al. (1987b) on the basis of interpreted Cretaceous magnetic anomalies. The oceanic reflection Moho is visible at 9.8 s close to the south end of the profile (Plate 2, km –990). Although oceanic crust cannot be traced inboard of the toe of the inferred accretionary wedge on this unmigrated profile, on nearby profiles a reflection can be traced to 12 s (Marlow and Cooper, 1985), a reflection we believe represents the top of oceanic crust frozen in the act of underthrusting the margin.

Crystalline basement and Moho. From the Saint Matthew–Nunivak Arch to the Beringian margin the lower crust lacks the laminated reflectivity so prominent around Saint Lawrence Island. Although changes in the lower crust are gradational, and the image of lower-crustal reflectivity constantly varies along the profile, we suggest that a change in crustal type or history is marked by the broad zone of weak reflections, dipping 15° to 20°N, that occupies the middle and lower crust from km –425 to –510. The reflection Moho is unclear over this region, but from km –500 to –600 is at 12 s to 13 s, indicating a crust that is either 10%–20% thicker, or has velocities that are 10%–20% slower, than in the central segment north of the Saint Matthew Basin. Upper-crustal refraction velocities from unreversed sonobuoys along a west-southwest–trending line south of Saint Matthew Island 200 km to the southeast (Fig. 1) reach 5.7–6.5 km/s at only 1–3 km depth, and 6.8–7.6 km/s at only 4–8 km depth (1.5–3 s) (Cooper et al., 1987). These high velocities seem to correlate with a gravity high that can be traced 200 km along strike to our profile at km –550 to –600 (Fig. 2; Klemperer et al., this volume, Chapter 19, their Fig. 3), where our reflection Moho is deepest, implying that the crust is of high density, as well as high velocity. The gravity model of Cooper et al. (1987) along their sonobuoy line shows a crust that reaches 43 km thickness. Although this estimate of 43 km is very dependent on the density contrast assumed at the crust-mantle boundary (e.g., Holliger and Klemperer, 1990), it is consistent with our observation of reflection Moho at 13 s if the average crustal velocity is 6.6 km/s.

The reflection Moho begins to shallow beneath the northern shoulder of the Navarin Basin, from 13 s at km –575 to 11 s at km –615, thereby demonstrating true crustal thinning beneath the little-subsided shoulder of the basin. Although the lower-

crustal image is poor below the deep basin, bright reflections at ~11 s may be from the Moho. This traveltime implies a Moho depth of 21–27 km subsurface (13–20 km below the red unconformity) depending on local basin thickness (4–8 km), assumptions about thickness of Cretaceous and Paleogene carapace strata (5–10 km), and the velocity of crystalline basement (6.0–6.6 km/s). This estimate may be compared to the gravity model of Cooper et al. (1987) that places Moho at 20–22 km. The reflection Moho is visible at 11.5 s beneath the relatively thin sedimentary cover (<1.5 s Neogene reflectors) of the Lisa Ridge (km –830) southwest of the Navarin Basin, and even deeper beneath the Saint Matthew–Nunivak Arch, northeast of the Navarin Basin. Basement has been thinned by a factor of at least 2, if we take these traveltimes to the reflection Moho adjacent to the Navarin Basin as estimates of the crustal thickness predating the basin, and based on traveltimes to the red unconformity of as much as 6 s (km –770). Although our seismic profile demonstrates clear crustal thinning and apparent normal faulting, areal fault patterns interpreted from datasets more extensive than our single two-dimensional transect have been used to suggest that the Navarin Basin formed by transtension (Worrall, 1991) along margin-parallel strike-slip faults.

DISCUSSION

In an attempt to summarize our new data and observations of the nature of continental crust along our transect, we next note the important general characteristics of the crust and mantle beneath this region. The variable character of lower-crustal and Moho reflectivity along our transect permits us to divide the continent into three parts. The central part has highly reflective crust, whereas the northern and southern parts are comparatively nonreflective within the crustal basement. By inference from onshore geology, we associate the northern region (Beaufort margin and Chukchi Shelf) with the Arctic Alaska–Chukotka block, the central region (Bering Strait and Inner Bering Shelf) with the reworked middle to Late Cretaceous magmatic belt, and the southern region (Outer Bering Shelf and Beringian margin) with a collage of Paleozoic and Mesozoic terranes and Paleogene arcs. An absence of reflectivity is always difficult to interpret, and a lack of lower-crustal reflections beneath deep basins is particularly difficult to distinguish from poor signal penetration. However, we use the presence of Moho reflections along most of our profile as an indication that where we see no lower-crustal reflections, our data are nonetheless adequate to deduce that the lower crust is relatively nonreflective rather than obscured by noise. We summarize our observations by comparing key seismic attributes of our three continental regions with the crustal signature of the nearby active Aleutian arc (Fig. 4) (McGeary et al., 1994).

The Aleutian reflection section (Fig. 4A) is characterized by bright intramantle reflections from the subducting Pacific slab (McGeary, 1997; Holbrook et al., 1999), but only sporadic lower crustal or Moho reflections (McGeary et al., 1994). Crustal velocity is high in the intraoceanic arc, especially in the lower crust that in some places may be gradational into the upper mantle (Fliedner and Klemperer, 1999). In the part of the Aleutian arc forming on older continental crust of the Alaskan Peninsula, both crustal velocity and crustal thickness are within the typical range of continental crust (Fliedner and Klemperer, 2000). The crust beneath the Alaska Peninsula formed by arc magmatism within terranes similar or identical to those believed to make up the Outer Bering Shelf, whereas the crust beneath the Aleutian Islands is that of a pristine intraoceanic arc. A comparison of the characteristics of the Aleutian arc with the characteristics of the Outer Bering Shelf helps us to interpret the nature of the southern segment of our transect.

Southern region: Paleogene arc and displaced terranes

Figure 4B cartoons the Navarin Basin above a nonreflective crust, and continentward-dipping, sub-Moho reflections as imaged beneath the inactive Beringian margin by Marlow and Cooper (1985). The lack of crustal reflectivity is consistent with reflection profiles across other intraoceanic arcs (the Aleutian intraoceanic arc; Fig. 4A; McGeary et al., 1994) and intracontinental arcs (the active Cascades arc, Keach et al., 1989; the Mesozoic Sierra Nevada, Nelson et al., 1986). The high average velocity of 6.6 km/s, which we tentatively derive by comparing the reflection and the gravity Mohos, exceeds that of mean continental crust (Christensen and Mooney, 1995), but is the same as found for the modern Aleutian oceanic arc in 30-km-thick crust (Fliedner and Klemperer, 1999). The larger thickness, ~40 km, is comparable to that of arcs such as the modern Aleutian intracontinental arc of the western Alaska Peninsula, in which part of the thickness is due to preexisting crust (Fliedner and Klemperer, 2000). Cooper et al. (1987) described the long-wavelength magnetic high that crosses our profile at ~km –550 (Fig. 2; Klemperer et al., this volume, Chapter 19, their Fig. 4) as similar to the anomaly pattern that occurs over the volcanic mass of the Aleutian Ridge, reinforcing our view that this southern region includes one or more arcs, presumably of late Mesozoic to early Tertiary age.

However, the region from the axis of the Saint Matthew–Nunivak arch to the modern shelf edge is far too broad to have formed by arc magmatism alone. It is 250–450 km wide and was ~40 km thick across the entire region before the formation of the Navarin Basin. At the crustal growth rates evidenced in the modern Aleutian arc, where a 200-km-wide arc of 25–30 km thickness grew in 55 Ma (Holbrook et al., 1999), the Outer Bering Shelf would require 100–180 Ma to be created by arc magmatism alone (and 2–4 times longer if we accept the much lower estimates of arc production rates of Reymer and Schubert, 1984), requiring arc initiation in this region at least as early as 155 Ma (Late Jurassic). The existence of the middle to Late Cretaceous Okhotsk–Chukotsk magmatic belt extending across the Bering Strait several hundred kilometers to the north further demonstrates that arc magmatism was not restricted to the re-

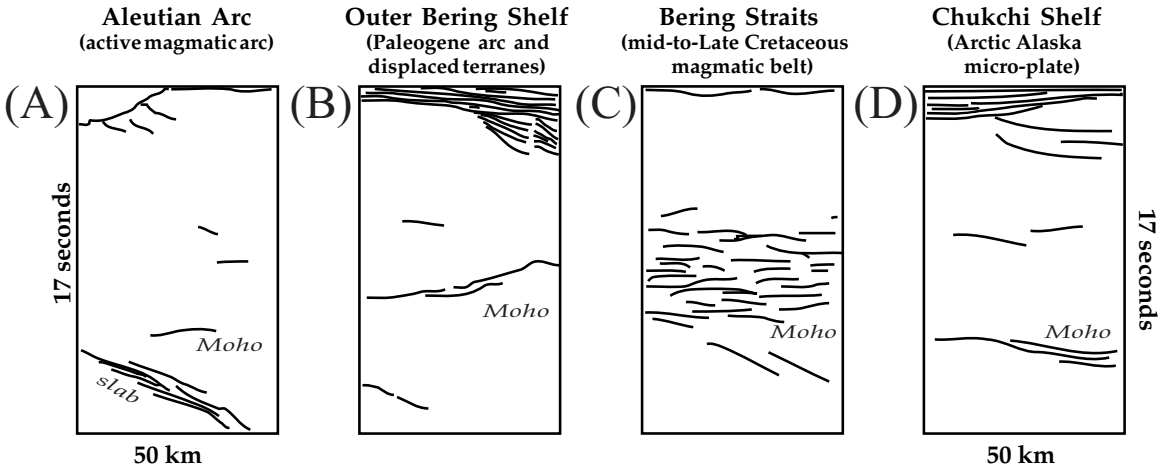

Upper-crustal velocity:	high (1, 2) ~ 6.5 km/s	probably high (4) 5.7 - 7.6 km/s	low (6) 5.8 - 6.1 km/s	low (6) 5.8 - 6.1 km/s
Lower-crustal velocity:	high (1, 2) ~ 7.0 km/s	probably high ≥6.6 km/s(?)	normal (6) 6.1 - 6.7 km/s	normal (6) 6.1 - 6.7 km/s
Lower-crustal reflectivity:	weak or absent (3)	poorly imaged	strongly layered	weak or absent
Reflection Moho:	sporadic (1, 3)	single band	base of layering	single band
Refraction Moho:	may be gradational (1)	not known	clearly defined	clearly defined
Mantle reflectors:	yes (3, 1)	probably (5)	yes	not known

Figure 4. Representative reflection characteristics, schematized in line drawings, from (A) active Aleutian arc (McGeary et al., 1994; McGeary, 1997); (B) Outer Bering Shelf (Navarin Basin, Plate 2); (C) Bering Strait and Inner Bering Shelf (near Saint Lawrence Island, Plate 2); (D) Arctic Alaska microplate (north margin of Colville foredeep and underlying Franklinian and older basin, Plate 2). Key velocity and reflectivity attributes of these crustal types are discussed in this chapter, or are taken from literature: (1) Fliedner and Klemperer (1999); (2) Holbrook et al. (1999); (3) McGeary et al. (1994); McGeary (1997); (4) Cooper et al. (1987); (5) Marlow and Cooper (1985); (6) Wolf et al. (this volume).

gion south of the Saint Matthew–Nunivak arch. Therefore, a large proportion of older crust must be present beneath the Outer Bering Shelf, into which the late Mesozoic to early Tertiary arc rocks were intruded. This older crust of unidentified allochthonous terranes may include the Peninsular terrane, which comprises largely Early Jurassic Talkeetna oceanic arc material (e.g., Plafker and Berg, 1994b), even though Peninsular terrane rocks have not been dredged as far west as our transect (Cooper et al., 1987; Worrall, 1991; see tabulation of dredge samples from the Beringian shelf edge in Plate 1, this volume). Paleogene arc magmatism constitutes an intrusive assemblage that has obliterated any distinctions between the different terranes beneath the Bering Shelf. Because Moho reflections are typically not clear beneath the modern Aleutian arc (McGeary et al., 1994; Fliedner and Klemperer, 1999), we speculate that the relatively sharp reflection Moho visible beneath the Navarin Basin developed after cessation of arc activity, and was created by the extension that formed that basin.

In Figure 2 we show a transitional change in lower-crustal reflectivity from the central mid-Cretaceous magmatic belt to the southern Late Cretaceous–Paleogene magmatic arc province. Cooper et al. (1987, p. 81) and Worrall (1991, p. 22) defined a broad region of "short-period, high-amplitude [magnetic] anomalies" that they suspected marks a "magmatic arc complex" and which on our transect spans the region from ~km –350 to –650 (Fig. 2). The northern and southern limits of the highest-amplitude magnetic anomalies along our transect are at the southern flank of the Saint Matthew Basin and northern flank of the Navarin Basin; however, the increasing thickness of sedimentary rocks, particularly to the south, probably suppresses the short-period magnetic anomalies. Short-period anomalies of gradually diminishing amplitude were recorded as far north as km –100 on our transect. Given that areal magnetic coverage is not complete in this region (Klemperer et al., this volume, Chapter 19, their Fig. 4), we only suggest the possibility that the gradual change in magnetic character may equate

with the transitional change in crustal reflectivity that we place at km –450 ± 50 km.

Central region: Middle to Late Cretaceous extensional and magmatic belt

Figure 4C cartoons the crust of the Inner Bering Shelf and the Bering Strait region, where crustal reflectivity is significantly greater than that beneath the Outer Bering Shelf. This characteristic lower-crustal reflectivity was first observed to be widespread in the thin crust of young extensional provinces across the UK continental shelf (e.g., Matthews and Cheadle, 1986) and in the western United States (Allmendinger et al., 1987), and was assumed to be due to extensional processes. Given later discovery of similar reflectivity in many cratonic regions (e.g., BABEL Working Group, 1990; Cook et al., 1999), it now appears probable that lower-crustal reflectors typically represent tectonically imposed layering, including shear zones (e.g., Green et al., 1990) and/or primary igneous layering produced by mafic intrusions into the lower crust (e.g., Warner, 1990). In any individual location it is difficult to distinguish between these possibilities, and large-magnitude extension is likely to be associated with both shearing and new intrusions. Other possible causes of deep-crustal reflectivity (e.g., primary depositional layering, metamorphic layering, and fluid-related phenomena) seem less likely to produce sufficiently strong reflections (e.g., Warner, 1990). Modest extension in the course of intracontinental basin formation (β factor <2) seems unlikely to create significant reflectivity because it produces little magmatism, only small rotation or transposition of preexisting layering, and minor development of new foliation (Nelson, 1991). Attention has therefore focused on extension (crustal collapse) during or after crustal thickening or postorogenic delamination and uplift as likely origins for much observed highly reflective crust worldwide (Warner, 1990; Nelson, 1992; Rey, 1993). In these tectonic settings abundant magmatism and large extension can combine to generate significant new crustal reflectivity.

The limited extension ($\beta = 1.5$) beneath the Hope, Norton, and Saint Matthew Basins shown by our reflection profiles suggests that this episode of Tertiary basin formation is not the source of the observed lower-crustal reflectivity. Instead we attribute the reflectivity of the Inner Bering Shelf and the Bering Strait to the postulated collapse of Mesozoic crust overthickened by crustal shortening during formation of the Brookian orogen, and by subsequent plutonism within the middle to Late Cretaceous magmatic belt (Rubin et al., 1995; Bering Strait Geologic Field Party, 1997). The observed region of reflective crust and uniform crustal thickness coincides with the locus of Cretaceous plutonism mapped on land. Studies on land in the Chukotka and Seward Peninsulas indicate that magmatic heating, metamorphism, and deformation during the time span 108–90 Ma (Miller et al., this volume, Chapter 17) likely affected the entire crustal column. The uniform thickness of 32 km beneath the Chukchi and Inner Bering shelves (Wolf et al., this volume) matches the global average thickness of extended continental crust of 31.5 km (Christensen and Mooney, 1995). The lower crust from Saint Lawrence Island to the Seward Peninsula has velocities in the range 6.5–6.7 km/s (Wolf et al., this volume) that are not consistent with the underplating of thick mafic units with velocities ~7 km/s. These velocities are consistent, however, with a bimodal crust consisting of ~6.5 km/s felsic to intermediate igneous and metamorphic lithologies intruded by ~7 km/s gabbroic sills. We presume such mafic sills are the source of the mafic xenoliths with cumulate textures (Wirth et al., this volume) and the 85–100 Ma ages of granulite facies crustal xenoliths (Miller et al., this volume, Chapter 10) found within younger lava flows on Saint Lawrence Island. Small-scale velocity variation between the suggested felsic to intermediate lower crust and mafic intrusions cannot be detected by our wide-angle data, which record only volumetric averages of the velocity, but we suggest that it is detected by the reflection data as the prominent reflectivity of the lower crust in this area (cf. Wenzel et al., 1987). However, the lower velocity of the middle crust, 6.1–6.4 km/s from 16 to 24 km depth (Wolf et al., this volume), precludes a large component of new mafic intrusions, and suggests that much of the reflectivity in this depth range must represent extensional fabrics formed in a ductile middle crust, such as are exposed in gneiss domes on the Chukotka and Seward Peninsulas (Fig. 1; Akinin and Calvert, this volume; Amato et al., this volume).

The low velocities of the upper crust (5.8–6.1 km/s to 16 km depth, Wolf et al., this volume) seem likely to represent Cretaceous granite, such as the granite that crops out at the surface on Saint Lawrence and the Diomede Islands and the paragneisses that crop out on Seward Peninsula (Christensen and Mooney, 1995). However, the moderate lower-crustal velocities imply that a voluminous mafic counterpart to the Cretaceous granites in the upper crust is not present today in the lower crust. Possibly a voluminous mafic counterpart never existed (which seems to require that the upper-crustal granites are crustal melts), or it formerly existed (according to Amato and Wright [1997] the granite is dominantly fractionated from mafic melt newly derived from the mantle by arc magmatism) but subsequently delaminated. Although Neogene and Quaternary basaltic volcanism (Akinin et al., 1997) presumably also left some traces within the crust, the basalts and their entrained xenoliths come directly from the mantle, and the proportion of mafic rocks intruded into the crust must be low because average crustal velocities here are close to the global continental crustal average of 6.4 km/s (Christensen and Mooney, 1995).

We conclude that the prominent lower-crustal reflectivity that characterizes the middle to Late Cretaceous magmatic belt was generated in part during magmatic thickening, but particularly by the ensuing extensional collapse and possible delamination. The magnitude of extension may have been greater in the Bering Strait, thinning the crust to the extent that it is now below sea level, than to the west or east, where gneiss domes produced by this extension rise 1 km above sea level. These gneiss

domes imply ~5 km thicker crust if their topography is supported by Airy isostasy, consistent with onshore crustal thickness measurements of 38 km along the TACT profile in the Koyukuk Basin immediately south of the Brooks Range (Fuis et al., 1995). Middle Cretaceous extension and middle to Late Cretaceous magmatism certainly affected the onshore areas of Alaska (Miller and Hudson, 1991; Miller et al., this volume, Chapter 17), and we interpret the reflective crust of the Yukon-Tanana terrane (Beaudoin et al., 1992) and of the Koyukuk Basin (Fuis et al., 1995) as having formed in the same manner and at the same time, as observed along our marine transect. The more complete collapse of the orogen in the Bering Strait segment could have been a consequence of local plate geometry, with rapid slab rollback in the Bering Strait region facilitated by the presence of an open ocean south of the subduction zone west of Alaska (Rubin et al., 1995), but precluded along strike to the east by continental terranes south of the subduction zone (Amato et al., this volume).

Northern region: Arctic Alaska microplate

In Figure 4D we show the character of the northern region as poorly reflective crust beneath deep basins and above a distinct reflection Moho. Comparing D to B in Figure 4, the superficial resemblance of Arctic Alaska crust to the crust of the Outer Bering Shelf cautions against a one-to-one assignment of specific seismic characteristics to particular tectonic environments. Whereas the reflectivity character of the Chukchi Shelf resembles that of the Outer Bering Shelf, the velocity structure of the Chukchi Shelf is nearly indistinguishable from that of the Bering Strait and Inner Bering Shelf (Wolf et al., this volume). The low upper-crustal velocities of the Chukchi Shelf (5.7–6.1 km/s to 15 km depth) presumably represent the thick sedimentary succession imaged on our reflection profiles, as opposed to the granite of similar seismic velocity on the Inner Bering Shelf. Nonetheless, specific reflectivity patterns appear to characterize, and hence may be used to map, specific crustal blocks (e.g., Klemperer et al., 1990; Brown, 1991), and we suggest that the sparse crustal reflectivity of the Arctic Alaska crust on our marine profiles also characterizes the crust beneath the allochthons of the northern Brooks Range (Fuis et al., 1995, their Fig. 2A).

The northern segment of our profile, beneath the Chukchi Shelf, is the most difficult to interpret, because the basement is not exposed, and because it has the longest history, >1 Ga. The Arctic Alaska microplate has undergone at least three extensional episodes, forming the Proterozoic to Franklinian basins, the Mississippian to Early Cretaceous south-facing Ellesmerian continental margin, and the modern north-facing Beaufort margin. In addition, localized extension apparently related to dextral slip on the Kobuk fault created the Hope Basin in the continental interior during the Paleogene. If the clear image of the reflection Moho beneath Arctic Alaska crust resulted from extension, then it is likely of different age in different regions, in part Tertiary (beneath the Hope Basin) and in part Jurassic or older (beneath the Ellesmerian and Franklinian basins). Whereas high topography requires that a crustal root still underlies the Brooks Range in Alaska (Fig. 1; Fuis et al., 1995), neither topography nor a root are present in the region of the Hope and Kotzebue Basins where crossed by our profiles (see also refraction-seismic and gravity evidence; Wolf et al., this volume). Though topography and a root can be inferred to have existed during and prior to the deposition of the mid-Cretaceous Corwin Delta of the Colville foredeep, they could have been destroyed by only relatively minor extension ($\beta \leq 1.5$), without creation of lower crustal reflectivity. However, unless crustal reflectivity beneath Arctic Alaska was destroyed following its creation (e.g., through disruption by dike injection over long periods of time; Nelson, 1991), the lack of intracrustal reflectivity suggests that northern Alaska never underwent orogenic thickening and postorogenic collapse of the style evidenced farther to the south. This conclusion, drawn from the lack of crustal reflectivity, is also demonstrated by the well-known continuity of Proterozoic and younger strata across Arctic Alaska that is clearly seen on our transect.

SUMMARY AND CONCLUSIONS

This first continuous deep-crustal reflection profile acquired across the entire North American continent provides baseline information on crustal thickness and evolution for the Alaskan continental shelves from the Aleutian Basin of the Bering Sea to the Canada Basin of the Arctic Ocean. Our profiles traverse many areas that are distant from onshore outcrop, so our interpretations, although building on a history of basin exploration on the Bering and Chukchi shelves, are inevitably broad. Our transect does, however, provide new insight into various aspects of continental growth and modification in Alaska and northeastern Russia, as recorded by crustal reflectivity patterns.

Our transect (Fig. 2) shows the central Bering Strait–Inner Bering Shelf basement high, flanked to north and south by large accumulations of Tertiary sediments at the modern shelf edges (Beaufort and Beringian margins) or interior to a narrow marginal high (Navarin Basin). In contrast, neither of the deep Tertiary sedimentary basins in the continental interior (Hope Basin beneath the Chukchi Shelf and Norton Basin beneath the Inner Bering Shelf) are rift basins, but rather seem to be accommodations of strike-slip faulting.

The observed gradual thickening of crystalline basement from the Proterozoic core of the Arctic Alaska–Chukotka plate to the Bering Strait (Fig. 2) may in part reflect the accretion and growth of continental crust to the south, the crust of the Bering Shelf being dominated by Phanerozoic components. The oldest crust beneath Arctic Alaska, extending southward in the subsurface beneath Brooks Range and Herald Arch thrusts, appears to have remained a relatively stable block or microplate since the Late Proterozoic, only mildly modified by the stretching, thrusting, and loading events along its southern margin produced by the Brookian orogeny. The preservation of a great thickness of

stratified sedimentary rocks beneath the Chukchi Shelf, above the thin crystalline basement of Arctic Alaska, is due to the long-term stability of Arctic Alaska, which has saved the older basins from being overprinted by younger events. It is uncertain whether this relative stability is due to crustal age or lithology, or whether it is a consequence of the distance of Arctic Alaska from the Mesozoic active-margin-related deformation.

The thicker basement of our central belt from the Seward Peninsula to south of Saint Lawrence Island was derived, at least in part, from the same Precambrian continental crust including Proterozoic to Paleozoic sedimentary successions, but also from magmatic accretion. The crust of this central belt represents a zone of former weakness in which the older crust was completely reworked at what was then the continental margin by Late Jurassic to early Late Cretaceous compression and thickening, followed by extension and magmatism, to create its present distinctive reflection character. This extension, we believe, expanded the area of central Alaska and its shelf southward and brought the topography of an overthickened crust back to near sea level. This tectonic reworking may represent one way in which the more juvenile crust of the Outer Bering Shelf could in the future acquire a more typical continental character through a similar sequence of orogenesis.

The Outer Bering Shelf is underlain by the youngest crust along our transect, and may be formed of assembled terranes of Mesozoic and older rocks that were intruded by Mesozoic and Cenozoic arc magmas. Perhaps accretionary events without substantial crustal shortening or thickening (i.e., Mediterranean-style orogens; Burchfiel and Royden, 1991), and/or translation of material along strike-slip faults into a region without major shortening, helped preserve a first-cycle crust with its original thickness and character, as seen beneath the Outer Bering Shelf. Although the major strike-slip faults that bound Alaskan terranes onshore have so far proved largely unrecognizable offshore, we can map divergent normal fault systems and crustal thinning beneath the offshore Hope and Norton Basins capable of accommodating the strain represented by two of these strike-slip faults, the Kobuk and Kaltag faults. We suggest that these faults continue west beneath our transect, albeit with progressively diminishing offset as their strike-slip displacement is transformed into extension beneath the shelf basins. Dominantly strike-slip (transpressional) accretion in the southern Bering Shelf contrasts with the collisional orogenesis and crustal thickening in the Brooks Range and the central zone of our transect. In the central zone, collisional accretion of Paleozoic and Mesozoic terranes with the preexisting sedimentary cover and Precambrian basement led inexorably to the subsequent modification of these terranes beyond easy recognition by the processes of crustal collapse, extension, and intrusion of magmas.

ACKNOWLEDGMENTS

This cruise was funded by the National Science Foundation Continental Dynamics grant EAR-93–17087; additional scientific participation and initial seismic processing were funded by the U.S. Geological Survey Deep Continental Studies Program. We thank the shipboard scientific staff, captain, and crew of the RV *Ewing* for their efforts in acquiring high-quality seismic data, and the staff of Scott Pickford for processing of the reflection data. Tom Brocher and Walter Mooney provided helpful reviews. University of Alaska, Fairbanks, and Royal Holloway, University of London, kindly hosted Klemperer during part of this work. All the reflection seismic data are available from Stanford University for the cost of reproduction.

REFERENCES CITED

Akinin, V.V., Roden, M.F., Francis, D., Apt, J., and Moll-Stalcup, E.J., 1997, Compositional and thermal state of the upper mantle beneath the Bering Sea basalt province: Evidence from the Chukchi Peninsula of Russia: Canadian Journal of Earth Sciences, v. 34, p. 789–800.

Allmendinger, R.W., Hauge, T.A., Hauser, E.C., Potter, C.J., Klemperer, S.L., Nelson, K.D., Knuepfer, P., and Oliver, J., 1987, Overview of the COCORP 40°N Transect, western United States: The fabric of an orogenic belt: Geological Society of America Bulletin, v. 98, p. 308–319.

Amato, J.M., and Wright, J.E., 1997, Petrogenesis of the potassic Kigluaik pluton: Arc-related mafic magmatism in northern Alaska: Journal of Geophysical Research, v. 102, p. 8065–8083.

BABEL Working Group, 1990, Evidence for Early Proterozoic plate tectonics from seismic reflection profiles in the Baltic Shield: Nature, v. 348, p. 34–38.

Barnes, D.F., Marianio, J., Morin, R.L., Roberts, C.W., and Jachens, R.C., 1994, Incomplete isostatic gravity map of Alaska, *in* Plafker, G., and Berg, H.C., eds., The geology of Alaska: Boulder, Colorado, Geological Society of America, Geology of North America, v. G-1, plate 9, scale 1:2 500 000, 1 sheet.

Beaudoin, B.C., Fuis, G.S., Mooney, W.D., Nokleberg, W.J., and Christensen, N.I., 1992, Thin, low-velocity crust beneath the southern Yukon-Tanana terrane, east-central Alaska: Results from TACT refraction/wide-angle reflection data: Journal of Geophysical Research, v. 97, p. 1921–1942.

Bering Strait Geologic Field Party, 1997, Koolen metamorphic complex, NE Russia: Implications for the tectonic evolution of the Bering Strait region: Tectonics, v. 16, p. 713–729.

Brocher, T.M., Allen, R.M., Stone, D.B., Wolf, L.W., and Galloway, B.K., 1995, Data report for onshore-offshore wide-angle seismic recordings in the Bering-Chukchi Sea, western Alaska and eastern Siberia: U.S. Geological Survey Open-File Report 95–0650, 57 p.

Brown, L.D., 1991, A new map of crustal "terranes" in the United States from COCORP deep seismic reflection profiling: Geophysical Journal International, v. 105, p. 3–13.

Campbell, R.H., 1967, Areal geology in the vicinity of the Chariot Site, Lisburne Peninsula, northwestern Alaska: U.S. Geological Survey Professional Paper 395, 71 p.

Christensen, N.I., and Mooney, W.D., 1995, Seismic velocity structure and composition of the continental crust: A global view: Journal of Geophysical Research, v. 100, p. 9761–9788.

Coflin, K.C., Cook, F.A., and Geis, W.T., 1990, Evidence for Ellesmerian convergence in the subsurface east of the Mackenzie Delta: Marine Geology, v. 93, p. 289–301.

Collins, F.R., 1958, Test wells, Topagoruk area, Alaska. 5. Subsurface geology and engineering data: Exploration of Naval Petroleum Reserve No. 4 and adjacent areas, northern Alaska, 1944–1953: U.S. Geological Survey Professional Paper 305-D, p. 265–316.

Collins, F.R., 1961, Core tests and test wells, Barrow area, Alaska. 5. Subsurface geology and engineering data: Exploration of Naval Petroleum Reserve No. 4 and adjacent areas, northern Alaska, 1944–1953: U.S. Geological Survey Professional Paper 305-K, p. 569–644.

Coney, P.J., and Jones, D.L., 1985, Accretion tectonics and crustal structure in Alaska: Tectonophysics, v. 119, p. 265–282.

Cook, F.A., van der Velden, A.J., Hall, K.W., and Roberts, B.J., 1999, Frozen subduction in Canada's Northwest Territories: Lithoprobe deep lithospheric reflection profiling of the western Canadian Shield: Tectonics, v. 18, p. 1–24.

Cooper, A.K., Marlow, M.S., and Scholl, D.W., 1987, Geologic framework of the Bering Sea crust, *in* Scholl, D.W., Grantz, A., and Vedder, J.G., eds., Geology and resource potential of the continental margin of western North America and adjacent ocean basins: Beaufort Sea to Baja California: Houston, Texas, Circum-Pacific Council for Energy and Mineral Resources, Earth Science Series, v. 6, p. 73–102.

Craig, J.D., Sherwood, K.W., and Johnson, P.P., 1985, Geologic report for the Beaufort Sea planning area, Alaska: Regional geology, petroleum geology, environmental geology: Anchorage, Alaska, U.S. Department of the Interior, Minerals Management Service Outer Continental Shelf Report 85–0111, 192 p.

Davis, A.S., Pickthorn, L.-B.G., Vallier, T.L., and Marlow, M.S., 1989, Petrology and age of volcanic-arc rocks from the continental margin of the Bering Sea: Implications for early Eocene relocation of plate boundaries: Canadian Journal of Earth Sciences, v. 26, p. 1474–1490.

Davis, A.S., Gunn, S.H., Gray, L.-B., Marlow, M.S., and Wong, F.L., 1993, Petrology and isotopic composition of Quaternary basanites dredged from the Bering Sea continental margin near Navarin Basin: Canadian Journal of Earth Sciences, v. 30, p. 975–984.

Dumitru, T.A., Miller, E.L., O'Sullivan, P.B., Amato, J.M., Hannula, K.A., Calvert, A.T., and Gans, P.B., 1995, Cretaceous to recent extension in the Bering Strait region, Alaska: Tectonics, v. 14, p. 549–563.

Eittreim, S., Grantz, A., and Whitney, O.T., 1978, Isopach maps of the Tertiary sediments, Hope Basin, southern Chukchi Sea, Alaska: U.S. Geological Survey Miscellaneous Field Studies Map MF-906, scale 1:1 000 000, 1 sheet.

Embry, A.F., 1990, Geological and geophysical evidence in support of the hypothesis of anticlockwise rotation of northern Alaska: Marine Geology, v. 93, p. 317–329.

Fisher, M.A., Patton, W.W., Jr., and Holmes, M.L., 1982, Geology of Norton Basin and continental shelf beneath northwestern Bering Sea, Alaska: American Association of Petroleum Geologists Bulletin, v. 66, p. 255–285.

Fliedner, M.M., and Klemperer, S.L., 1999, Composition of an island-arc: Wide-angle studies in the eastern Aleutian islands, Alaska: Journal of Geophysical Research, v. 104, p. 10667–10694.

Fliedner, M.M., and Klemperer, S.L., 2000, Crustal structure transition from oceanic arc to continental arc, eastern Aleutian Islands and Alaska Peninsula: Earth and Planetary Science Letters, v. 179, p. 567–579.

Fuis, G.S., Levander, A.R., Lutter, W.J., Wissinger, E.S., Moore, T.E., and Christensen, N.I., 1995, Seismic images of the Brooks Range, Arctic Alaska, reveal crustal-scale duplexing: Geology, v. 23, p. 65–68.

Fujita, K., and Newberry, J.T., 1982, Tectonic evolution of northeastern Siberia and adjacent regions: Tectonophysics, v. 89, p. 337–357.

Grantz, A., and May, S.D., 1987, Regional geology and petroleum potential of the United States Chukchi Shelf north of Point Hope, *in* Scholl, D.W., Grantz, A., and Vedder, J.G., eds., Geology and resource potential of the continental margin of western North America and adjacent ocean basins: Beaufort Sea to Baja California: Houston, Texas, Circum-Pacific Council for Energy and Mineral Resources, Earth Science Series, v. 6, p. 37–58.

Grantz, A., Wolf, S.C., Breslau, L., Johnson, T.C., and Hanna, W.F., 1970, Reconnaissance geology of the Chukchi Sea as determined by acoustic and magnetic profiling, *in* Adkison, W.L., and Brosge, M.M., eds., Proceedings of the Geological Seminar on the North Slope of Alaska: American Association of Petroleum Geologists, Pacific Section, Los Angeles, p. F1–F28.

Grantz, A., May, S.D., and Dinter, D.A., 1987, Regional geology and petroleum potential of the United States Beaufort and northeasternmost Chukchi Seas, *in* Scholl, D.W., Grantz, A., and Vedder, J.G., eds., Geology and resource potential of the continental margin of western North America and adjacent ocean basins: Beaufort Sea to Baja California: Houston, Texas, Circum-Pacific Council for Energy and Mineral Resources, Earth Science Series, v. 6, p. 17–35.

Grantz, A., May, S.D., and Hart, P.E., 1990, Geology of the Arctic continental margin of Alaska, *in* Grantz, A., Johnson, G.L., and Sweeney, J.F., eds., The Arctic Ocean region: Boulder, Colorado, Geological Society of America, Geology of North America, v. L, p. 257–288.

Grantz, A., Moore, T.E., and Roeske, S., 1991, Centennial continent/ocean transect #15: Gulf of Alaska to Arctic Ocean: Boulder, Colorado, Geological Society of America, 1:500 000, 3 sheets, 72 p. text.

Grantz, A., Clark, D.L., Phillips, R.L., and Srivastava, S.P., 1998, Phanerozoic stratigraphy of Northwind Ridge, magnetic anomalies in the Canada Basin, and the geometry and timing of rifting in the Amerasia Basin, Arctic Ocean: Geological Society of America Bulletin, v. 110, p. 801–820.

Green, A.G., Milkereit, B., Percival, J.A., Davidson, A., Parrish, R.R., Cook, F.A., Geis, W.T., Cannon, W.F., Hutchinson, D.R., West, G.F., and Clowes, R.M., 1990, Origin of deep crustal reflections: Seismic profiling across high-grade metamorphic terranes in Canada: Tectonophysics, v. 173, p. 627–638.

Hatton, L., Worthington, M.H., and Makin, J.E., 1986, Seismic data processing: Theory and practice: Oxford, UK, Blackwell Science Publishers, 177 p.

Higgins, A.K., Ineson, J.R., Peel, J.S., Surlyk, F., and Sønderholm, M., 1991, Cambrian to Silurian basin development and sedimentation, North Greenland, *in* Trettin, H.P., ed., Geology of the Innuitian Orogen and Arctic Platform of Canada and Greenland: Ottawa, Canada, Geological Survey of Canada, Geology of Canada, no. 3, p. 109–161.

Holbrook, W.S., Lizarralde, D., McGeary, S., Bangs, N., and Diebold, J., 1999, Structure and composition of the Aleutian island arc and implications for continental crustal growth: Geology, v. 27, p. 31–34.

Holliger K., and Klemperer, S.L., 1990, Gravity and deep seismic reflection profiles across the North Sea rifts, *in* Blundell, D.J., and Gibbs, A.D., Tectonic evolution of the North Sea rifts: Oxford, UK, Oxford University Press, p. 82–100.

Holmes, M.L., and Creager, J.S., 1981, The role of the Kaltag and Kobuk faults in the tectonic evolution of the Bering Strait region, *in* Hood, D.W., and Calder, J.A., eds., The eastern Bering Sea Shelf: Oceanography and resources: Boulder, Colorado, National Oceanic and Atmospheric Administration, Department of Commerce, v. 1, p. 293–302.

Houtz, R.E., Eittreim, S., and Grantz, A., 1981, Acoustic properties of northern Alaska shelves in relation to the regional geology: Journal of Geophysical Research, v. 86, p. 3935–3943.

Jin, D.J., and Herrin, E., 1980, Surface wave studies of the Bering Sea and Alaska: Bulletin of the Seismological Society of America, v. 70, p. 2117–2144.

Jones, D.L., Silberling, N.J., and Hillhouse, J.W., 1977, Wrangellia: A displaced terrane in northwestern North America: Canadian Journal of Earth Sciences, v. 14, p. 2565–2577.

Jones, D.M., Kingston, M.J., Marlow, M.S., Cooper, A.K., Barron, J.A., Wingate, F.H., and Arnal, R.E., 1981, Age, mineralogy, physical properties, and geochemistry of dredge samples from the Bering Sea continental margin: U.S. Geological Survey Open-File Report 81–1297, 68 p.

Kanasewich, E.R., and Berkes, Z., 1990, Seismic structure of the Proterozoic on Melville Island, Canadian Arctic archipelago: Marine Geology, v. 93, p. 421–448.

Keach, R.W., II., Oliver, J.E., Brown, L.D., and Kaufman, S., 1989, Cenozoic active margin and shallow Cascades structure: COCORP results from western Oregon: Geological Society of America Bulletin, v. 101, p. 783–794.

Kirschner, C.E., 1988, Map showing sedimentary basins of onshore and continental shelf areas, Alaska: U.S. Geological Survey Map I-1873, scale 1:5 000 000, 1 sheet.

Kirschner, C.E., 1994, Interior basins of Alaska, *in* Plafker, G., and Berg, H.C., eds., The geology of Alaska: Boulder, Colorado, Geological Society of America, Geology of North America, v. G-1, p. 469–493.

Klemperer, S.L., 1989, Processing BIRPS deep seismic reflection data: A tutorial review, *in* Cassinis, R., Nolet, G., and Panza, G.F., eds., Digital seismology and fine modeling of the lithosphere: New York, Plenum Press, Et-

tore Majorana International Science Series, Physical Sciences, v. 42, p. 229–257.

Klemperer, S.L., and Hobbs, R.W., 1991, The BIRPS atlas: Deep seismic reflection profiles from around the British Isles: Cambridge, Cambridge University Press, 124 p., 99 sections.

Klemperer, S.L., and Hurich, C.A., 1990, Lithospheric structure of the North Sea from deep seismic reflection profiling, *in* Blundell, D.J., and Gibbs, A.D., eds., Tectonic evolution of the North Sea rifts: Oxford, UK, Oxford University Press, p. 37–63.

Klemperer, S.L., Hauge, T.A., Hauser, E.C., Oliver, J.E., and Potter, C.J., 1986, The Moho in the northern Basin and Range province, Nevada, along the COCORP 40°N seismic-reflection transect: Geological Society of America Bulletin, v. 97, p. 603–618.

Klemperer, S.L., Hobbs, R.W., and Freeman, B., 1990, Dating the source of lower crustal reflectivity using BIRPS deep seismic profiles across the Iapetus suture: Tectonophysics, v. 173, p. 445–454.

Lane, L.S., 1997, Canada Basin, Arctic Ocean: Evidence against a rotational origin: Tectonics, v. 16, p. 363–387.

Lawver, L.A., and Scotese, C.R., 1990, A review of tectonic models for the evolution of the Canada Basin, *in* Grantz, A., Johnson, G.L., and Sweeney, J.F., eds., The Arctic Ocean region: Boulder, Colorado, Geological Society of America, Geology of North America, v. L, p. 593–618.

Lerand, M., 1973, Beaufort Sea, *in* McCrossan, R.G., ed., The future petroleum provinces of Canada: Their geology and potential: Canadian Society of Petroleum Geologists Memoir 1, p. 315–386.

Mackey, K.G., Fujita, K., Gunbina, L.V., Kovalev, V.N., Imaev, V.S., Koz'min, B.M., and Imaeva, L.P., 1997, Seismicity of the Bering Strait region: Evidence for a Bering Block: Geology, v. 25, p. 979–982.

Mackey, K.G., Fujita, K., and Ruff, L.J., 1998, Crustal thickness of northeast Russia: Tectonophysics, v. 284, p. 283–297.

Marlow, M.S., and Cooper, A.K., 1980, Mesozoic and Cenozoic structural trends under southern Bering Sea Shelf: American Association of Petroleum Geologists Bulletin, v. 64, p. 2139–2155.

Marlow, M.S., and Cooper, A.K., 1985, Regional geology of the Beringian continental margin, *in* Nasu, N., ed., Formation of active ocean margins: Boston, Massachusetts, Terra Scientific Publishing, p. 497–515.

Marlow, M.S., Scholl, D.W., Cooper, A.K., and Buffington, E.C., 1976, Structure and evolution of Bering Sea Shelf south of St. Lawrence Island: American Association of Petroleum Geologists Bulletin, v. 60, p. 161–183.

Marlow, M.S., Cooper, A.K., and Fisher, M.A., 1987, Petroleum geology of the Beringian continental shelf, *in* Scholl, D.W., Grantz, A., and Vedder, J.G., eds., Geology and resource potential of the continental margin of western North America and adjacent ocean basins: Beaufort Sea to Baja California: Houston, Texas, Circum-Pacific Council for Energy and Mineral Resources, Earth Science Series, v. 6, p. 103–122.

Matthews, D.H., and Cheadle, M. J., 1986, Deep reflections from the Caledonides and Variscides west of Britain and comparison with the Himalayas, *in* Barazangi, M., and Brown, L.D., eds., Reflection seismology: A global perspective: American Geophysical Union Geodynamics Series, v. 13, p. 5–19.

Mayfield, C.F., Tailleur, I.L., and Ellersieck, I., 1988, Stratigraphy, structure, and palinspastic synthesis of the western Brooks Range, northwestern Alaska, *in* Gryc, G., ed., Geology and exploration of the National Petroleum Reserve in Alaska, 1974 to 1982: U.S. Geological Survey Professional Paper 1399, p. 143–186.

McGeary, S., 1997, The deep seismic reflection image of the Aleutian subducting plate as an analog for other mantle reflectors: Geological Society of America Abstracts with Programs, v. 29, no. 6, p. 233.

McGeary, S.E., and Ben-Avraham, Z., 1981, Allochthonous terranes in Alaska: Implications for the structure and evolution of the Bering Shelf: Geology, v. 9., p. 608–613.

McGeary, S., Diebold, J.B., Bangs, N.L., Bond, G., and Buhl, P., 1994, Preliminary results of the Pacific to Bering Shelf deep seismic experiment: Eos (Transactions, American Geophysical Union), v. 75, no. 44, supplement, p. 643.

McKerrow,W.S., MacNiocaill, C., and Dewey, J.F., 2000, The Caledonian orogeny redefined: Journal of the Geological Society, London, v. 157, p. 1149–1154.

Meissner, R., 1986, The continental crust: A geophysical approach: Orlando, Florida, Academic Press, International Geophysics Series, v. 34, 426 p.

Miller, E.L., and Hudson, T.L., 1991, Mid-Cretaceous extensional fragmentation of a Jurassic–Early Cretaceous compressional orogen, Alaska: Tectonics, v. 10, p. 781–796.

Moll-Stalcup, E.J., 1994, Latest Cretaceous and Cenozoic magmatic rocks of Alaska, *in* Plafker, G., and Berg, H.C., eds., The geology of Alaska: Boulder, Colorado, Geological Society of America, Geology of North America, v. G-1, plate 5, 1:2 500 000, 1 sheet.

Moll-Stalcup, E.J., Brew, D.A., and Vallier, T.L., 1994, Latest Cretaceous and Cenozoic magmatism in mainland Alaska, *in* Plafker, G., and Berg, H.C., eds., The geology of Alaska: Boulder, Colorado, Geology of North America, v. G-1, p. 589–619.

Mooney, W.D., and Brocher, T.M., 1987, Coincident seismic reflection/refraction studies of the continental lithosphere: A global review: Geophysical Journal of the Royal Astronomical Society, v. 89, p. 1–6.

Moore, T.E., Wallace, W.K., Bird, K.J., Karl, S.M., Mull, C.G., and Dillon, J.T., 1994, Geology of northern Alaska, *in* Plafker, G., and Berg, H.C., eds., The geology of Alaska: Boulder, Colorado, Geological Society of America, Geology of North America, v. G-1, p. 49–140.

Nelson, K.D., 1991, A unified view of craton evolution motivated by recent deep seismic reflection and refraction results: Geophysical Journal International, v. 105, p. 25–35.

Nelson, K.D., 1992, Are crustal thickness variations in old mountain belts like the Appalachians a consequence of lithospheric delamination?: Geology, v. 20, p. 498–502.

Nelson, K.D., Zhu, T.F., Gibbs, A., Harris, R., Oliver, J.E., Kaufman, S., Brown, L., and Schweickert, R.A., 1986, COCORP deep seismic reflection profiling in the northern Sierra Nevada, California: Tectonics, v. 5, p. 321–333.

Nokleberg, W.J., Parfenov, L.M., Monger, J.W.H., Norton, I.O., Khanchuk, A.I., Stone, D.B., Scotese, C.R., Scholl, D.W., and Fujita, K., 2000, Phanerozoic tectonic evolution of the circum-North Pacific: U.S. Geological Survey Professional Paper 1626, 122 p.

Ostenso, N.A., 1968, A gravity survey of the Chukchi Sea region, and its bearing on westward extension of structures in northern Alaska: Geological Society of America Bulletin, v. 79, p. 241–254.

Patton, W.W., Jr., and Csejtey, B., Jr., 1980: Geologic map of St. Lawrence Island, Alaska: U.S. Geological Survey, Miscellaneous Investigations Series I-1203, scale 1:250 000, 1 sheet.

Patton, W.W., Jr., Lanphere, M.A., Miller, T.P., and Scott, R.A., 1976, Age and tectonic significance of volcanic rocks on St. Matthew Island, Bering Sea, Alaska: Journal of Research of the U.S. Geological Survey, v. 4, p. 67–73.

Patton, W.W., Jr., Box, S.E., Moll-Stalcup, E.J., and Miller, T.P., 1994, Geology of west-central Alaska, *in* Plafker, G., and Berg, H.C., eds., The geology of Alaska: Boulder, Colorado, Geological Society of America, Geology of North America, v. G-1, p. 241–269.

Pavlis, T.L., Sisson, V.B., Foster, H.L., Nokleberg, W.J., and Plafker, G., 1992, Mid-Cretaceous extensional tectonics of the Yukon-Tanana terrane, Trans-Alaska Crustal Transect (TACT), east-central Alaska: Tectonics, v. 12, p. 103–122.

Peddy, C., Brown, L.D., and Klemperer, S.L., 1986, Interpreting the deep structure of rifts with synthetic seismic sections: American Geophysical Union Geodynamics Series, v. 13, p. 301–311.

Plafker, G., and Berg, H.C., editors, 1994a, The geology of Alaska: Boulder, Colorado, Geological Society of America, Geology of North America, v. G-1, 1055 p.

Plafker, G., and Berg, H.C., 1994b, Overview of the geology and tectonic evolution of Alaska, *in* Plafker, G., and Berg, H.C., eds., The geology of Alaska: Boulder, Colorado, Geological Society of America, Geology of North America, v. G-1, p. 989–1021.

Rey, P., 1993, Seismic and tectonometamorphic characters of the lower continental crust in Phanerozoic areas: A consequence of post-thickening extension: Tectonics, v. 12, p. 580–590.

Reymer, A., and Schubert, G., 1984, Phanerozoic addition rates to the continental crust and growth: Tectonics, v. 3, p. 63–77.

Rickwood, F.K., 1970, The Prudhoe Bay field, *in* Adkison, W.L., and Brosge, M.M., eds., Proceedings of the Geological Seminar on the North Slope of Alaska: American Association of Petroleum Geologists, Pacific Section, Los Angeles, p. L1–L11.

Rubin, C.M., Miller, E.L., and Toro, J., 1995, Deformation of the northern circum-Pacific margin: Variations in tectonic style and plate-tectonic implications: Geology, v. 23, p. 897–900.

Scholl, D.W., and Stevenson, A.J., 1989, The Aleutian-Bowers-Shirshov arc system, response to deformation of Alaska ("orocline") by subduction-driven impact and escape of crustal masses: Exploration of an idea: Eos (Transactions, American Geophysical Union), v. 70, no. 43, p. 1307.

Scholl, D.W., Marlow, M.S., Creager, J.S., Holmes, M.L., Wolf, S.C., and Cooper, A.K., 1970, A search for the seaward extension of the Kaltag Fault beneath the Bering Sea: Geological Society of America Abstracts with Programs, v. 2, no. 2, p. 141–142.

Scholl, D.W., Grantz, A., and Vedder, J.G., editors, 1987a, Geology and resource potential of the continental margin of western North America and adjacent ocean basins: Beaufort Sea to Baja California: Houston, Texas, Circum-Pacific Council for Energy and Mineral Resources, Earth Science Series, v. 6, 799 p.

Scholl, D.W., Vallier, T.L., and Stevenson, A.J., 1987b, Geologic evolution and petroleum geology of the Aleutian Ridge, *in* Scholl, D.W., Grantz, A., and Vedder, J.G., eds., Geology and resource potential of the continental margin of Western North America and adjacent ocean basins: Beaufort Sea to Baja California: Houston, Texas, Circum-Pacific Council for Energy and Mineral Resources, Earth Science Series, v. 6, p. 123–155.

Sherwood, K.W., 1992, Stratigraphy, structure and origin of the Franklinian, Northeast Chukchi Basin, Arctic Alaska Plate, *in* Thurston, D.K., and Fujita, K., eds., Proceedings of the 1992 International Conference on Arctic Margins: Anchorage, Alaska, Minerals Management Service, p. 245–250.

Shumway, G., Moore, D.G., and Dowling, G.B., 1964, Fairway Rock in Bering Strait, *in* Miller, R.L., Papers in marine geology, Shepard Commemorative Volume: New York, Macmillan, p. 401–407.

Stockwell, C.H., McGlynn, J.C., Emslie, R.F., Sanford, B.V., Norris, A.W., Donaldson, J.A., Fahrig, W.F., and Currie, K.L., 1970, Geology of the Canadian Shield, *in* Douglas, R.J.W., ed., Geology and economic minerals of Canada: Geological Survey of Canada, Economic Geology Report, v. 1, p. 44–150.

Sweeney, J.F., Mayr, U., Sobczak, L.W., and Balkwill, H.R., 1986, North American Continent-Ocean Transects Program, Transect G: Canadian Arctic: Somerset Island to Canada Basin: Boulder, Colorado, Geological Society of America, Centennial Continent/Ocean Transect no. 11, scale 1:500 000, 2 sheets.

Thurston, D.K., and Theiss, L.A., 1987, Geologic report for the Chukchi Sea planning area, Alaska: Regional geology, petroleum geology, and environmental geology: Anchorage, Alaska, U.S. Department of the Interior, Minerals Management Service Outer Continental Shelf Report 87–0046, 193 p.

Till, A.B., and Dumoulin, J.A., 1994, Geology of Seward Peninsula and St. Lawrence Island, *in* Plafker, G., and Berg, H.C., eds., The geology of Alaska: Boulder, Colorado, Geological Society of America, Geology of North America, v. G-1, p. 141–152.

Till, A.B., Box, S.E., Roeske, S.M., and Patton, W.W., Jr., 1993, Comment on "Mid-Cretaceous extensional fragmentation of a Jurassic-Early Cretaceous compressional orogen, Alaska": Tectonics, v. 12, p. 1076–1086.

Tolson, R.B., 1987a, Structure and stratigraphy of the Hope Basin, southern Chukchi Seas, Alaska, *in* Scholl, D.W., Grantz, A., and Vedder, J.G., eds., Geology and resource potential of the continental margin of western North America and adjacent ocean basins: Beaufort Sea to Baja California: Houston, Texas, Circum-Pacific Council for Energy and Mineral Resources, Earth Science Series, v. 6, p. 59–71.

Tolson, R.B., 1987b, Structure, stratigraphy, tectonic evolution and petroleum source potential of the Hope Basin, southern Chukchi Sea, Alaska [Ph.D. thesis]: Palo Alto, California, Stanford University, 261 p.

Trettin, H.P., 1991, Summary: Silurian–Early Carboniferous deformational phases and associated metamorphism and plutonism, Arctic Islands, *in* Trettin, H.P., ed., Geology of the Innuitian Orogen and Arctic Platform of Canada and Greenland: Boulder, Colorado, Geological Society of America, Geology of North America, v. E, p. 337–341.

Trettin, H.P., Mayr, U., Long, G.D.F., and Packard, J.J., 1991, Cambrian to Early Devonian basin development, sedimentation, and volcanism, Arctic Islands, *in* Trettin, H.P., ed., Geology of the Innuitian Orogen and Arctic Platform of Canada and Greenland: Ottawa, Canada, Geological Survey of Canada, Geology of Canada, no. 3, p. 163–238.

Turner, R.F., McCarthy, C.M., Steffy, D.A., Lynch, M.B., Martin, G.C., Sherwood, K.W., Flett, T.O., and Adams, A.J., 1984, Geological and operational summary, Navarin Basin COST No. 1 well, Bering Sea, Alaska: Anchorage, Alaska, U.S. Department of the Interior, Minerals Management Service Outer Continental Shelf Report 84–0031, 245 p.

Turner, R.F., Martin, G.C., Flett, T.O., and Steffy, D.A., 1985, Geologic report for the Navarin Basin planning area, Bering Sea, Alaska: Anchorage, Alaska, U.S. Department of the Interior, Minerals Management Service Outer Continental Shelf Report 85–0045, 140 p.

Turner, R.F., Martin, G.C., Flett, T.O., and Steffy, D.A., 1986, Geologic report for the Norton Basin planning area, Bering Sea, Alaska: Anchorage, Alaska, U.S. Department of the Interior, Minerals Management Service Outer Continental Shelf Report 86–0033, 179 p.

Warner, M.R., 1990, Basalts, water, or shear zones in the lower continental crust?: Tectonophysics, v. 173, p. 163–174.

Warner, M., Morgan, J., Barton, P., Morgan, P., Price, C., and Jones, K., 1996, Seismic reflections from the mantle represent relict subduction zones within the continental lithosphere: Geology, v. 24, p. 39–42.

Wenzel, F., Sandmeier, K.-J., and Wälde, W., 1987, Properties of the lower crust from modeling refraction and reflection data: Journal of Geophysical Research, v. 92, p. 11575–11583.

Wirth, K.R., and Bird, J.M., 1992, Chronology of ophiolite crystallization, detachment, and emplacement: Evidence from the Brooks Range, Alaska: Geology, v. 20, p. 75–78.

Worrall, D.M., 1991, Tectonic history of the Bering Sea and the evolution of Tertiary strike-slip basins of the Bering Shelf: Geological Society of America Special Paper 257, 120 p.

Yilmaz, O., 1987, Seismic data processing: Tulsa, Oklahoma, Society of Exploration Geophysicists, Investigations in Geophysics, v. 2, 526 p.

Manuscript Accepted by the Society May 15, 2001.

Printed in the U.S.A.

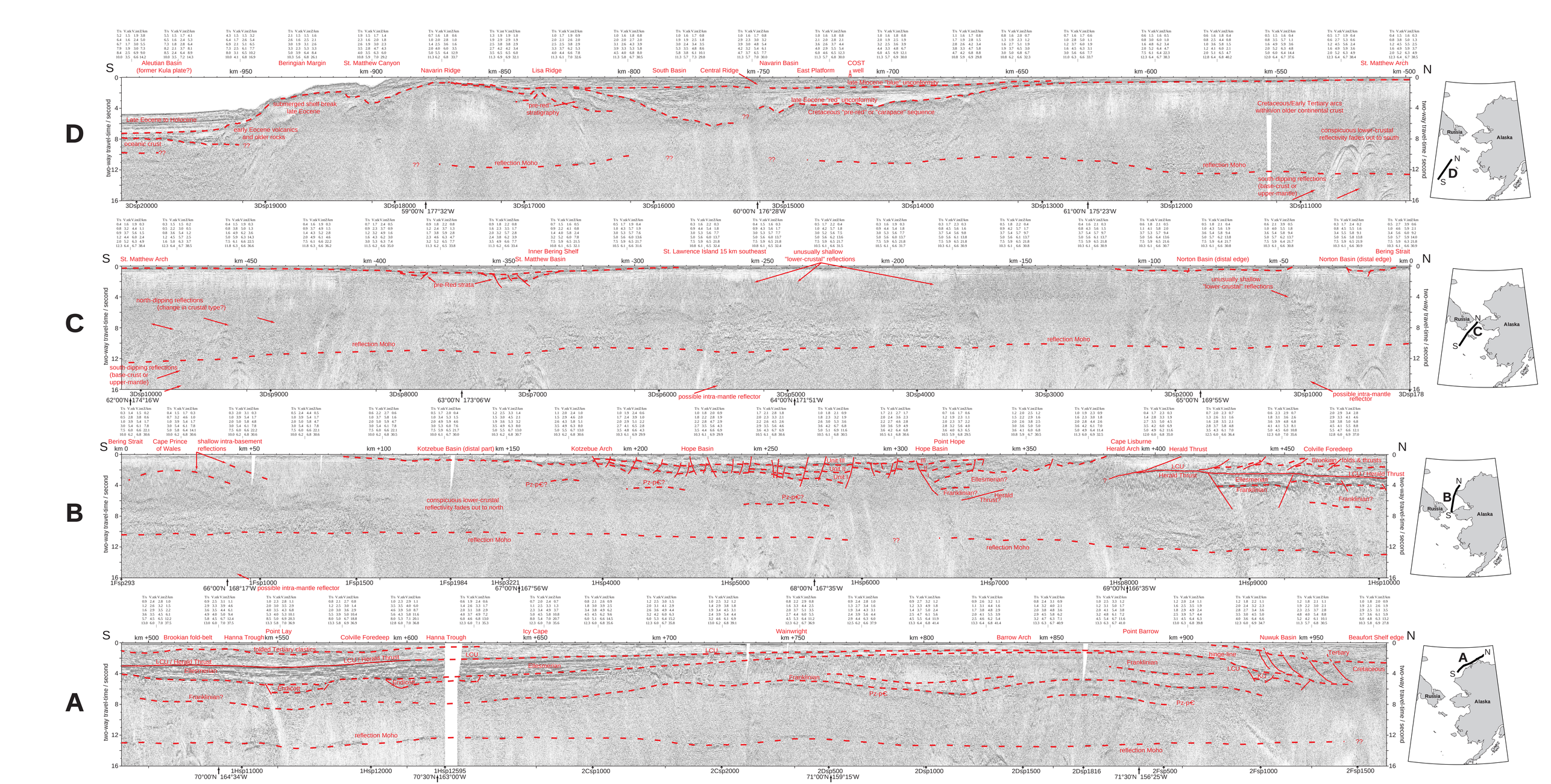

Plate 1.
Seismic data along profile S-N in figure 1, and as shown in line-drawing format in figure 2.
Display scale is 1:400,000, with no vertical exaggeration at a velocity of 6 km/s.
Line location: From Aleutian Basin 58°00'N 178°30'W (top panel) (50 m shot-spacing, 17 sec record length) to Navarin Ridge 59°00'N 177°32'W to COST Well 60°11'N 176°16'W to (upper middle panel) St. Lawrence Island, Northwest Cape 63°55'N 172°00'W to dog-leg around Russian waters 65°27'N 169°03'W to Bering Strait 65°35'N 168°51'W. Line of section offset 25 km to east. From Bering Strait 65°35'N 168°18'W (lower middle panel) (75 m shot spacing, 18 or 20 sec record length) to Diomede Island 66°00'N 168°17'W to (change in recording parameters to 50 m shot-spacing, 16 sec record length at 67°10'N 167°54'W) to Pt. Hope 68°00'N 167°35'W to Cape Lisburne 69°00'N 166°35'W to (bottom panel) Pt. Lay 70°00'N 164°35'W to Icy Cape 70°30'N 163°00'W to (change in recording parameters to 75 m shot spacing, 18 or 20 sec record length at 70°51'N 160°09'W) Wainwright 70°52'N 160° 00'W to Barrow 71°34'N 156°00'W to end of line at ice edge at 71°49'N 154°33'W. Refer to figure 1 for approximate line locations, and to Plate 1 accompanying the preface to this volume (Grantz and others, this vol.) for precise locations. The top two panels comprise line 3D shotpoints 20133 to 178, and the lower two panels 1F shotpoint 293 to 1G shotpoint 350 and line 1H 3221 to 2F shotpoint 1646. Shot-point numbers are annotated every 1000 in general (e.g. 3Dsp20000 = line segment 3D, shot-point 20000).

Velocity information derived from the reflection data is shown above the seismic data at c. 25 km, intervals. T/s is the two-way travel time in seconds at which the stacking velocity (V.stk) was applied during processing. Because of space limitations, time-velocity-depth information is only given for six travel-times at each location, even though it was measured and applied at up to 20 times at each location. V.int is the Dix interval velocity for the layer immediately above the travel-time and depth shown and Z/km = depth calculated from these interval velocities. Interval velocities and depths shown were calculated from the complete list of stacking velocities derived at each location, not from just the six shown here, with the assumption that the stacking velocities (processing velocities) are equal to the root-mean-square (rms) velocities for the earth. Because stacking velocities are chosen to give the optimum stack, by correctly stacking primary reflections including dipping reflections and by reducing the effect of multiples and side-swipe, stacking velocities are often somewhat larger than the true rms velocity (e.g. Hatton and others (1986); Klemperer (1989)). Hence, the calculated interval velocities and depths also tend to be somewhat larger than the true interval velocities and depths.

Acquisition parameters: A Digicon DMS-2000 system recorded output of a digital 160-channel streamer, 4 km in length, with 25-meter hydrophone spacing, towed at a nominal depth of 15 m. The near and far receiver offsets were 200 m and 4175 m. The source was a 8355 in^3 (137.7 l), 20-chamber airgun array. The navigation system was a Magnavox MX-4200D Global Positioning System and Ashtech 3D CPS with speed log information provided by a FURUNO CI-30 three-axis, doppler speed log/current profiler. 3.5 kHz depth-sounder records, gravity and magnetic data are available from Lamont-Doherty Earth Observatory, Columbia University, mggdb@lamont.ldeo.columbia.edu. An Atlas Hydrosweep 3.5 kHz depth-sounder logged every second. A Bell Aerospace BGM-3 marine gravity meter logged every second, and a Varian V75 magnetometer logged every 6 seconds. Wide-angle records from the 12 wide-angle recording stations operational during the marine seismic profiling (Figure 1; Brocher et al., 1995) are freely available from IRIS Data Management Center through http://www.iris.edu. The geophones were typically Mark Products L-28, 3-component 4.5 Hz instruments. Additionally, four dozen Sparton Electronics 53B/8W62 disposable sonobuoys were deployed from the R/V Ewing during the cruise, at fairly regular intervals, providing refraction data to offsets of c. 20 km.

Processing sequence: Pre-stack processing (by Scott-Pickford, Inc.):
1. Input SEG-Y 8 ms data.
2. Apply geometry: 50 m (75 m) source interval, 25 m receiver interval.
3. Edit noisy traces.
4. Apply gain: T**1.8 to 9 s only.
5. Apply NMO (guessed function); apply AGC (500 ms window).
6. F-K filter, remove dips > ± 14 ms/trace, with 15 point taper.
7. Remove AGC; remove NMO.
8. Minimum phase bandpass filter: 2/4 – 40/50 Hz.
9. Predictive deconvolution in two windows, shallow window: 304 ms operator, 32 ms gap length; deep window: 400 ms operator, 48 ms gap length.
10. Sort to CMP domain.
11. Apply NMO. Velocities picked at 6 km intervals from semblance analysis, moved-out gathers and mini-stacks.
12. First-break mute: 300 m / 0 ms; 400 m / 350 ms; 600 m / 700 ms; 1000 m / 1700 ms; 1400 m / 2250 ms; 4200 m / 5000 ms.
13. Inside mute: 187 m / 700 ms; 612 m / 4200 ms; 620 m / 17000 ms.
14. Edit spikes.
15. Apply dip move-out (DMO).
16. Stack, 40 fold (27 fold for 75-m source-point data) in 12.5 m CMP bins.

Post-stack processing for display (by Stanford and USGS):
17. Sub-sample to 16 ms with anti-alias filter.
18. FX-Decon with 1 sec window x 40-trace window.
19. Automatic gain control, 1500 ms window.
20. Predictive deconvolution in two windows: shallow operator length 256 ms, gap 32 ms, design window 0.5-4s, apply window 0 to 5 s; deep operator length 304 ms, gap 48 ms, design window 6-11s, apply window 5 to 16 s.
21. Mix adjacent traces 1:1:1, and sum four traces to 50 m CMPs.
22. Bandpass filter: 0-4 s, low pass 20 Hz stop 28 Hz, 4-8 s, low pass 15 Hz stop 22 Hz; 8-16 s, low pass 10 Hz stop 16 Hz.
23. Display 75 traces/cm horizontally, 0.8 cm/second vertically (scale 1:400,000, with no vertical exaggeration at a velocity of 6 km/s).
A description of these standard processing steps can be found in textbooks such as by Hatton et al. (1986) or Yilmaz (1987), and the testing procedures are described by Klemperer (1989).